JESTT

Vol. 1, Issue 2, 2024

SCOPUA

Journal of Engineering, Science and Technological Trends

ISSN(e): 2959-1937

Volume 1 (Issue 2) Published on 2024-08-31

https://doi.org/10.48112/jestt.v1i2c

Journal Homepage

https://journals.scopua.com/index.php/JESTT

Publisher

Scientific Collaborative Online Publishing Universal Academy

Publisher Homepage

https://scopua.com/

Model Town - Ferozepur Road, Near Atfaq Hospital, Lahore, Pakistan

Journal of Engineering, Science and Technological Trends

Aims and Scope

The Journal of Engineering, Science and Technological Trends (JESTT) is a double-blind-peer-reviewed, open-access wide-ranging journal for publishing novel primary research findings, reviews, and short communications throughout the broad gamut of engineering disciplines. The journal editorial board welcomes manuscripts in both fundamental and applied research areas and encourages submissions that contribute novel and innovative insights to engineering science and technology.

All submitted articles considered suitable for JESTT are subjected to rigorous double-blind peer review to ensure the highest levels of quality. The journal is highly interdisciplinary and welcomes scientifically robust research in traditional and emerging areas. Original papers which provide an essential contribution to the development of engineering sciences and report on significant developments in the field are encouraged. The review process is carried out as quickly as possible to minimize any delays in the online publication of articles.

JESTT aims to advance the understanding of engineering sciences by providing a platform for the publication of unique contributions in the field of engineering and technology across various topics, including, but not limited to, the Topics listed on our website. Its objectives are to provide a high-level forum for the dissemination and sharing of cutting-edge advances in engineering research and development, current primary research outputs, and significant accomplishments; to report progress in engineering science, to discuss trending topics, areas of interest, obstacles, and prospects in engineering development, and to take into account the well-being of people and the environment as well as engineering ethics; to promote engineering breakthroughs and innovations that benefit people and the environment.

Contents (Volume 1 & Issue 2 – 2024)

Journal of Engineering, Science and Technological Trends (JESTT)
Vol. 1, Issue 2, August 2024
DOI: https://doi.org/10.48112/jestt.v1i2c.1

Article

An Insight into Optical Constants of Iron Phenanthroline Molecules

Hayder Fahim[1&2*], Hashim Jabbar[1] and Adil A. Al-Fregi[1]

[1]University of Basrah, College of Science, Iraq

[2]Kerbala University, College of Education for Pure Science, Iraq

* Corresponding Email: hyder.fahem@uokerbala.edu.iq (H. Fahim)

Received: 07 November 2023 / Revised: 11 July 2024 / Accepted: 17 July 2024 / Published Online: 31 August 2024

ABSTRACT

In this study, we investigate the optical properties of Iron 1,10-phenanthroline molecular nanolayer synthesized were prepared using the complexation reactions method. Fe^{2+}(Phen) molecular thin films were then prepared as samples and subsequently characterized using XRD and UV-Vis spectroscopy. The main objective of this work is to explore the optical constants relevant to the light-induced spin crossover phenomenon in this molecule. UV-Vis study of nanometer thickness layer (100 nm) at wavelength $(200 - 1100\ nm)$, the distribution of refractive index is discussed in the framework of the single oscillator Wemple-DiDomenico model and various distribution parameters such as single oscillator energy (E_o), dispersion energy (E_d), refractive index ($n_{(0)}$), and optical absorption based on absorption edges dielectric constant (ε_∞) using Miller's rule. The moment of the dielectric constant optical spectrum (M_{-1}, M_{-3}) and energy gap by Wemple-DiDomenico approximation (E_g^{WDD}) have been computed, as has non-linear optical susceptibility ($\chi^{(3)}$), direct energy gap by Tauc relation (E_g^T), and Urbach energy of the localized states (E_u).

Keywords*:* Fe^{2+}(Phen) Molecular; Iron 1; 10-phenanthroline; Ligand Exchange Synthesis Method; Spin Crossover Phenomenon

1. Introduction

The photophysical characteristics of $Fe(II)$ complexes containing polyimine ligands, such as $[(Fe(phen)_3]^{2+}$ $(phen = 1{,}10 - phenanthroline)$, have recently gained considerable attention [1]. These investigations are fundamentally important for understanding photophysics in $3D$ transition metal complexes, but they also have applications in comprehending optical writing/magnetic reading in spin crossover (SCO) compounds [2]. Furthermore, such compounds were considered as possible replacements for $Grätzel - type$ dye-sensitized photovoltaic cells [3]. Indeed, these diamagnetic low-spin d^6diimine complexes are thought to be models for $Fe(II)$ SCO complexes with N_6 coordination spheres based on heteroaromatic ligands. In comparison, SCO complexes typically have a substantially lower zero-point energy differential H_{HL} $(1000\ cm^{-1})$ between the $high - spin\ (HS)$ and $low - spin\ (LS)$ configurations with low ligand-field (LF) strength [4],[5]. The Light-Induced Excited Spin State Trapping $(LIESST)$ phenomenon is known for SCO complexes in which the low temperature LS ground state can be photoconverted to a long-lived metastable HS state in the solid state [6],[7]. It was previously demonstrated that such photoconversion might occur in solution at roughly room temperature utilizing pulsed irradiation and associated rapid relaxations [8]. Despite possessing a significantly higher H_{HL} $(6000\ cm^{-1})$, $Fe(II)$ LS polyimine complexes display the same conversion to a metastable HS state by ultrafast optical pumping, with even quicker matching relaxations [1],[4],[6] While these compounds have many intriguing optical properties, their usage in optics is currently limited due to the centrosymmetry that most $Fe(II)$ complexes with polyimine ligands have in solid state. This centrosymmetry precludes these compounds from showing fascinating features such as piezoelectric and electro-optic effects, as well as second order non-linear optical phenomena resulting in second harmonic and sum frequency creation. To broaden the use of $Fe(II)$ complexes, their inherent centrosymmetry must be broken [9],[10].

2. Experimental Part

Iron (II) complexes derived 1,10-phenanthroline (d^6) are arguably the most well-studied examples of spin-crossover

compounds due to the large change in magnetism that results from transitions between the low-spin, diamagnetic (S = 0) state to a high-spin (S = 2) state. So, in the present study, we will prepare three low spin- F(II) complexes containing both nitrogen and sulfur donor atoms with the general formula $[Fe(phen)_x(SCN)_y]_{c+}$ {x= 0, 1, 2, 3; y=0, 2, 4} and examined the spin crossover of these complexes.

A solution of ascorbic acid (approximately 10 g diluted in 20 mL of distilled water) was added drop by drop to the ferrous sulfate solution to create fresh $FeSO_4.7H_2O$. After the colour of the solution was changed to a light blue, the solution was allowed to cool to room temperature. After that, 20 mL of ethanol was added to afford ferrous sulfate hydrate $FeSO_4.7H_2O$ as light blue in 95% yield.

2.1. Preparation of bis (phenanthroline) dithiocyanatoiron (II) $Fe(Phen)_2(SCN)_2$

A solution (0.468 g, 2 mmol) of 1,10-phenanthroline hydrochloride monohydrate, in 20 mL of distilled water was added drop by drop to an aqueous solution of (0.278 g, 1 mmol), ferrous sulfate heptahydrate, in 15 mL of distilled water with gentle stirring. The mixture was stirred at room temperature for 3 hours. Then, a solution of 0.152 g, 2 mmol) of ammonium thiocyanate, NH_4SCN, was added. The reaction mixture was stirred for 3 hours to obtain a dark red colour which was then collected by filtration. The crude solid was washed several times with distilled water and ethanol to obtain red crystals of bis (phenanthroline) dithiocyanatoiron(II) $[Fe(Phen)_2(SCN)_2]$ in an 89% yield.

2.2. Preparation of Tris(phenanthroline) iron(II) sulfate $[Fe(Phen)_3]SO_4$

A mixture of light blue crystals of (0.278 g, 1 mmol) ferrous sulfate heptahydrate, $FeSO_4$ .7H2O and (0.702 g, 3 mmol) 1,10-phenanthroline hydrochloride monohydrate, in 25 mL of distilled water was stirred at room temperature for 3 hours. A red solution was formed which was then, reduced by a rotary evaporator to obtain a red solid. The crude solid was washed several times with ethanol to obtain red crystals of tris(phenanthroline)iron(II) sulfate in 93% yield.

2.3. Preparation of ammonium phenanthrolinetetra thiocyanatoferrate(II) $(NH_4)_2[Fe(Phen)(SCN)_4]$

A solution of 1,10-phenanthrolinium hydrochloride monohydrate, (0.234 g, 1 mmol) in 20 mL of distilled water was added slowly and drop by drop to the aqueous solution of ferrous sulfate heptahydrate, (0.278 g, 1 mmol), in 15 mL of distilled water. The mixture was stirred at room temperature for 1 hour. Then, a solution of ammonium thiocyanate, NH_4SCN, (0.304 g, 4 mmol) was added. The reaction mixture was stirred for 3 hours to obtain a dark red color solution which was then dried by rotary evaporator to dryness. The crude solid was washed several times with ethanol red crystals of ammonium phenanthroline tetra thiocyanato ferrate (II) $(NH_4)_2[Fe(Phen)(SCN)_4]$ in 77% yield.

2.4. Preparation of Ammonium hexathiocyanatoferrate(II) $(NH_4)_4[Fe(SCN)_6]$

A solution of (0.456 g, 6 mmol) ammonium thiocyanate in 20 mL of distilled water was added to an aqueous solution of (0.278 g, 1 mmol), ferrous sulfate heptahydrate, in 25 mL of distilled water with gentle stirring at room temperature for 3 hours. A darkened colour solution was obtained and then dried by a rotary evaporator to dryness. The crude solid was washed several times with ethanol to obtain red crystals of ammonium hexahiocyanatoferrate (II) $(NH_4)_4[Fe(SCN)_6]$ of about 92% yield.

2.5. Layer thin films of phenanthroline molecular using spin-coating

1- Fe $(phen)_2$ $(SCN)_2$ have been dissolved in ethanol to make a concentration of 0.1-1.0 mM.
2- The substrate was cleaned using ultrasonication for 10 min, Acetone, Ethanol, and N_2 gun.
3- solution was dropped onto the substrate, during rotation at 2000-4000 rpm for 30-60 s.
4- The samples were dried under a vacuum for 1–2 h to evaporate the solvent and to form a uniform thin film.

Optimization of preparation conditions such as solvent selection, concentration, spin speed, and duration can affect the properties of the thin film. The glass was employed as a substrate to create a thin film of the mentioned materials with a thickness of 100 nm, thickness was measured with a profilometer [F20-FilMetrics], and absorbance, transmittance, and reflectivity were measured by UV-Vis spectrophotometer. [Shimazdu - (UV-1800) - (1100-190) nm- Physics department/ Basrah University].The structural and optical characteristics of iron (phen) thin films were examined with $X-ray$ diffraction(XRD).

3. Results and discussion

The phase formation investigation was performed using an $XPERT-PRO\ X-ray$ diffractometer (XRD) with $Cu-K\alpha$ radiation ($\lambda = 1.54$ Å) over the range $2\theta \sim 10-80°$ with a step size of 0.02° . The results of $X-ray$ diffraction of $iron\ (phen)$ thin films were shown the crystal structure revealed by XRD of the SCO films at room temperature, it should be mentioned that the JCPD card for $Fe(phen)_2(SCN)_2$, $(NH_4)_2[Fe(phen)(SCN)_4]$, $(NH_4)_4[Fe(SCN)_6]$, and $[Fe(phen)_3]SO_4$ molecules is not available in the literature.

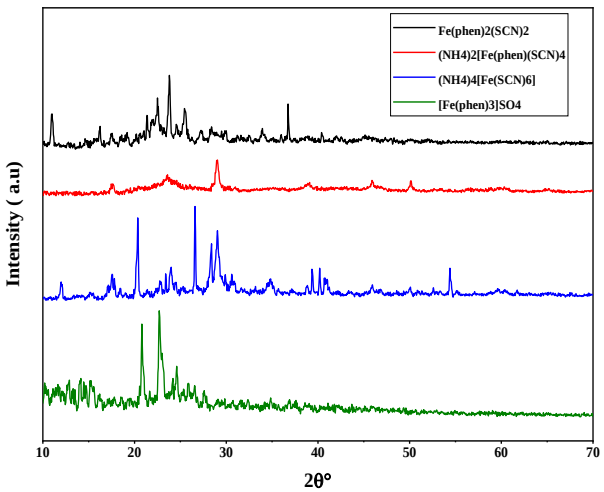

Figure 1: *The X-ray diffraction (XRD) pattern illustrating the diffraction behaviour of nanocrystals within the Fe (phen) thin films. This diffraction occurred on glass substrates at room temperature and a thickness of 100 nm.*

The XRD pattern in (Figure 1) provides information about the crystal structure of the thin films. By comparing the obtained diffraction peaks with the selection of Bragg peaks from Table 1

for different complexes, we can deduce the crystallographic phase present in the Fe(phen) thin films. Here's an explanation of the results based on the provided Table 1:

1. $Fe(phen)_2(SCN)_2$: The average crystal size is approximately 33.16 Å. The diffraction peak positions at various 2θ angles correspond to specific crystallographic planes within the $Fe(phen)_2(SCN)_2$ complex. The multiple peaks observed suggest that the thin film contains a crystalline phase with well-defined crystallographic orientations.

2. $(NH_4)_2[Fe(phen)(SCN)_4]$: The average crystal size is about 18.62 Å. The observed diffraction peaks correspond to specific crystallographic planes within the (NH4)2[Fe(phen)(SCN)4] complex. These peaks indicate the presence of a distinct crystalline structure in the thin film.

3. $(NH_4)_4[Fe(SCN)_6]$: The average crystal size is approximately 32.43 Å. The observed diffraction peaks align with specific crystallographic planes of the (NH4)4[Fe(SCN)6] complex. These peaks indicate the presence of a certain crystalline arrangement within the thin film.

4. $[Fe(phen)_3]SO_4$: The average crystal size is around 37.93 Å. The diffraction peaks observed at specific 2θ angles correspond to crystallographic planes within the [Fe(phen)3]SO4 complex. These peaks suggest the presence of a distinct crystalline phase within the thin film.

In summary, the XRD pattern reveals the presence of well-defined crystallographic phases in the Fe(phen) thin films, which correspond to the different complexes mentioned. The diffraction peaks and their positions provide insights into the arrangement of atoms within the crystal lattice of the thin films[11].

Table 1:
Selection of Bragg peaks extracted from X-ray diffractograms

Complexes	Average crystallite size (XRD) (nm)	The diffraction peak position (2θ°)
$Fe(phen)_2(SCN)_2$	33.16	11.02, 13.41, 14.70, 16.22, 17.55, 19.22, 21.40, 22.10, 22.55, 23.82, 24.62, 25.53, 27.27, 28.44, 29.08, 29.90, 32.53, 33.99, 36.02, 36.80, 38.83, 40.48, 42.17, 45.45
$(NH_4)_2[Fe(phen)(SCN)_4]$	18.62	17.60, 23.60, 29.03, 38.97, 45.96, 50.15, 59.97, 65.00
$(NH_4)_4[Fe(SCN)_6]$	32.43	12.06, 13.97, 15.30, 17.63, 18.47, 20.36, 21.41, 22.86, 23.44, 24.00, 25.31, 26.63, 28.37, 29.05, 30.72, 34.79, 38.84, 39.43, 40.23, 40.90, 46.00, 50.05, 54.46, 59.88
$[Fe(phen)_3]SO_4$	37.93	10.35, 11.56, 12.85, 14.08, 14.50, 15.25, 20.84, 22.75, 24.63, 25.89, 26.57, 27.62, 36.90, 38.88

Through the application of the Scherrer equation, the association is expressed as follows: (τ = (K * λ) / (β * Cos(θ)), wherein: τ stands for the nanoparticle's size. K represents a dimensionless constant, contingent on the crystal's shape, often falling within the range of about 0.9. β signifies the apex width at the mean height. θ corresponds to the Bragg angle. Lastly, λ denotes the wavelength, measured in nanometers [12].

The ligand and the iron complex both play crucial roles in terms of absorbance due to their interaction with light. The ligand contains specific functional groups that can absorb light at certain wavelengths, leading to distinct absorption bands in the spectrum. On the other hand, the iron complex can also contribute to absorbance as the central iron ion and its surrounding structure can influence the energy levels of electrons, causing them to absorb light at particular wavelengths. In essence, both the ligand and the iron complex contribute to the overall absorbance spectrum through their unique electronic properties and interactions with photons.The interaction between electromagnetic radiation and a thin film's material during absorption results in changes in the absorption spectra. These spectra provide information about the electronic configurations of the material and can be analyzed using UV-Vis absorption for studying electron-radiation interactions. Alternatively, infrared absorption is frequently employed to investigate the interaction between bond vibration energy and electromagnetic waves.

Within this context, the absorption (A) and the transmittance (T) spectra for $Fe(phen)$ thin films were recorded in the wavelength range of $(200 - 1100nm)$. The reflection (R) can be determined using the following relation[13]:

$$T = \frac{(1-R)^2 e^{-\alpha d}}{1-R^2 e^{-2\alpha d}} \qquad (1)$$

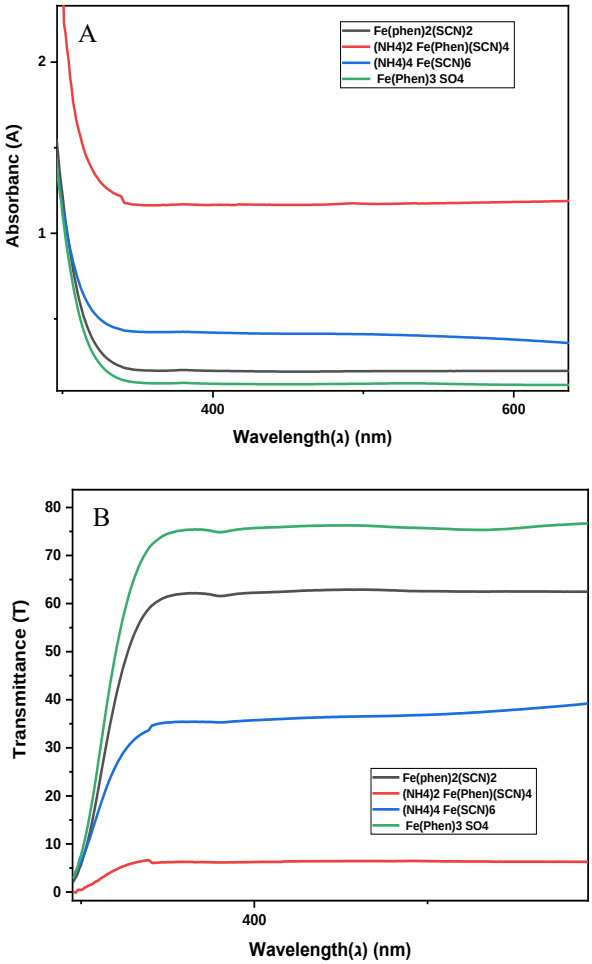

Figure 2: *The relationship between A- absorbance wavelength, B-transmittance and wavelength for Fe (phen) thin films at thickness 100 nm.*

Where T is transmittance, $\propto$ is the absorption coefficient, and d is the thickness of the sample. From the absorption coefficient data, extinction coefficient (K) can be calculated by:

$$K = \frac{\alpha\lambda}{4\pi} \qquad (2)$$

The refractive index (n) can be calculated using the following relation:

$$R = \frac{(n-1)^2+K^2}{(n+1)^2+K^2} \qquad (3)$$

Absorbance is a measure of how much light a material absorbs at a specific wavelength. In the context of the Fe (phen) thin films, the absorbance plot (A) illustrates how the films interact with light of different wavelengths. The molecular structure of the films and the electronic energy levels of their components play a crucial role in these interactions. When light passes through the thin films, it can be absorbed by the molecules present in the films. This absorption occurs due to electronic transitions, where electrons within the molecules are excited from lower energy levels to higher energy levels by absorbing photons of specific energies corresponding to certain wavelengths. The energy difference between these levels matches the energy of the incoming photons.

In the absorbance plot, peaks and valleys indicate the wavelengths at which these electronic transitions are most likely to occur. A peak represents a wavelength where the thin films absorb light most strongly because it corresponds to an energy level difference that matches the energy of the photons. These peaks are characteristic of the electronic structure of the molecules within the films.

Transmittance measures the fraction of light that passes through a material without being absorbed. In the transmittance plot (B), higher values indicate that the thin films are allowing more light to pass through, while lower values suggest that the films are absorbing more light. The relationship between absorbance and transmittance is complementary. If a material absorbs a significant amount of light at a certain wavelength (high absorbance), it will have low transmittance at that wavelength. Conversely, if a material absorbs very little light at a certain wavelength (low absorbance), it will have high transmittance at that wavelength. In the context of the Fe (phen) thin films, regions of high absorbance correspond to regions of low transmittance, and vice versa. The peaks in the absorbance plot align with the valleys in the transmittance plot. This indicates that the thin films are absorbing light strongly at those wavelengths, leading to reduced transmission of light through the films.

In summary, the absorbance and transmittance plots in Figure 2 provide a detailed picture of how the Fe (phen) thin films interact with light. The peaks in absorbance signify electronic transitions within the molecules, while the valleys in transmittance indicate regions where the films are absorbing light. Together, these plots offer insights into the molecular and electronic properties of the thin films.

The refractive index of a material, which can be determined using UV-visible absorption spectra, characterizes the path of light through the material as shown in Figure 3. A higher refractive index leads to greater deviation of light within the material. This optical constant is of great importance in the design of optical devices and provides key information about the material's optical properties, including its local field, polarization, and phase velocity of light. Refractive index:

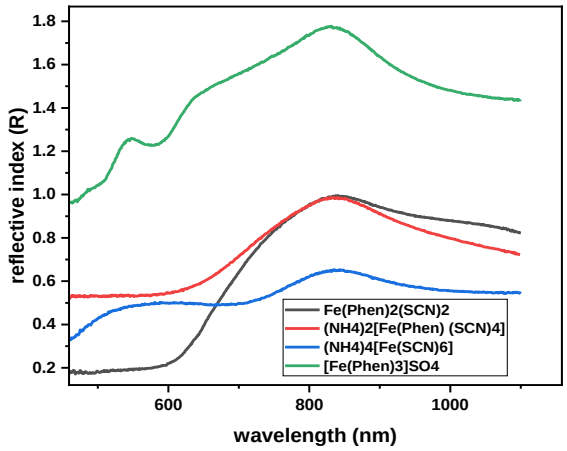

Figure 3: *The relationship between reflective index (R) and wavelength for Fe (phen)thin films at thickness 100 nm.*

$$\boldsymbol{n = \frac{1}{T_s} + \sqrt{\frac{1}{T_s - 1}}} \qquad (4)$$

Where $T_s = 10^{-A} * 100$, n : Refractive index, T_s=Transmittance, A: Absorbance. Now we have to plot a graph that shows variation in refractive index as a function of wavelength of light.

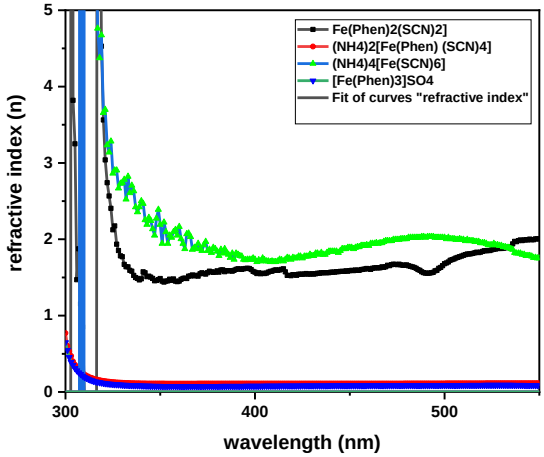

Figure 4: *The relationship between refractive index (n) and wavelength (λ) for thickness 100 nm, The symbols represent the experimental outcomes, while the solid lines depict the model fit data using the Sell Meier dispersion function.*

This graph shows that the refractive index initially decreases and then increases to its maximum value. After approaching this peak value, again it decreases. The observed distortion is attributed to the influence of the glass on the absorption edge around the wavelength of 300 nm and its adjacent region.

Figure 4 illustrate the refractive index values for different wavelengths (λ), which are commonly used to describe the optical properties of solids. The complex dielectric function $\varepsilon(E) = \varepsilon_1(E) + i\varepsilon_2(E)$, is a crucial tool for understanding these properties, as it provides frequency-dependent information about both the real part ε_1 and imaginary part ε_2. The quantity ε_2 is particularly significant, as it captures physical information about the material, including interband transitions at high energies $E \gg E_g$, interband transitions near the absorption edge, free carrier

absorption, and optical phonon absorption. The real part of the dielectric constant is the sum of these contributions, with K being negligible in the transparent region, leading to normal dispersion [14]. According to the single oscillator model, the dielectric constant (ε_1) dispersion is caused solely by interband transition and assumes that each electron acts as an oscillator [15]. Therefore, the dielectric constant (ε_1) can be expressed as:

$$\varepsilon_1(\omega) = 1 + \frac{F}{E_o^2 - (\hbar\omega)^2} \qquad (5)$$

The dielectric constant of a material can be calculated using the Wemple-DiDomenico model (WDD), which defines the parameter F as $F=E_dE_o$, where $E_d$represents dispersion energy and $E_o$represents single-oscillator energy. This model is based on the single-oscillator approximation, where E_o and F are parameters determined by the electric dipole oscillator. Thus, the dielectric constant can be expressed as a function of these parameters, as given in equation [16],[17].

$$\varepsilon_1(\omega) = n^2(\omega) - 1 = \frac{E_oE_d}{E_o - (\hbar\omega)^2} = \frac{E_d}{E_o}\left[1 - \frac{(\hbar\omega)^2}{E_o^2}\right]^{-1} \qquad (6)$$

The strength of interband optical transition and the chemical bonding in the unit cell are closely related to the dispersion energy E_d. On the other hand, the dispersion parameter E_d is commonly considered an "average" energy gap (E_g^{WDD}) and is empirically correlated with the lowest direct Tuac energy gap (E_g^T). The dispersion parameters E_o and E_d are determined using the r^{th}moment of the optical spectrum $\boldsymbol{\varepsilon_2(E)}$. The r^{th} moment of the $\boldsymbol{\varepsilon_2(E)}$spectrum can be defined as per [15][17]:

$$M_r = \frac{2}{\pi}\int_{E_t}^{\infty} E^r \varepsilon_2(E)dE \qquad (7)$$

Here, $E = \hbar\omega$ and E_t represents the energy threshold for absorption. Relationships between the dispersion parameters and $\boldsymbol{\varepsilon_2}$ (ω) spectrum can be established through:

$$E_o^2 = \frac{M_{-1}}{M_{-3}} \qquad (8)$$

$$E_d^2 = \frac{M_{-1}^3}{M_{-3}} \qquad (9)$$

Where $M_{-1}$and M_{-3} represent the moments of the optical spectrum, and the -1 and -3 moments are used to calculate E_o and E_d [16]. The static dielectric constant of any material is defined as:

$$\varepsilon_r(o) = \mathrm{Lim}_{E\to o} n^2(E) = n_o^2$$

The static dielectric constant can be expressed in terms of the dispersion parameters as follows:

$$n_o^2 = \varepsilon_r(o) = 1 + \frac{E_d}{E_o} \qquad (10)$$

The values of E_o andE_d can be obtained by plotting $(n^2 - 1)^{-1}$ against $(h\nu)^2$ and finding the gradient $(E_dE_o)^{-1}$ and the intercept (E_o/E_d) on the vertical axis, as illustrated in Figure 8. Table 1 provides the values of E_o, E_d, M_{-1}, M_{-3}, $n(o)$, and $\boldsymbol{\varepsilon}(\infty)$.$E_o$represents the distance between the centres of the valance and conduction bands. The Wemple-DiDomenico model can also be used to calculate the value of E_g^{WDD}, which is listed in Table 2. In the visible, nonlinear, and near-infrared regions, the Muller rule is a useful tool for equalizing the third-order nonlinear polarizability parameter ($\chi^{(3)}$) according to Wagner et al.[18], using the equation [16] :

$$\chi^{(3)} = A\left(\chi^{(1)}\right)^4 = A[E_oE_d/4\pi(E_o^2 - (h\nu)^2]^4 = \frac{A}{(4\pi)^4(n^2-1)^4} \qquad (11)$$

Where: $A = 1.7x10^{-10}$. **Figure 5** illustrates the third-order nonlinear optical susceptibilities for thicknesses of Fe (phen) thin films, which were calculated using equation (11).

Studying the optical absorption spectrum is a simple and effective method to explore the band structure of semiconducting materials. It involves analyzing the changes in transmitted light intensity with wavelength, which can reveal quantum mechanical transitions that electrons in the semiconductor may undergo. By doing so, researchers can gain insights into the distribution of allowed electronic energy levels. The Tauc relation [19] is commonly used to analyze the strong absorption region, where α increases linearly with increasing photon energy, and it provides a relationship between the absorption coefficient and photon energy. This relationship allows researchers to extract crucial information such as the band gap energy and Tauc exponent, which can provide details about the type of semiconductor, degree of disorder, or presence of impurities/defects [20].

$$\alpha h\nu = B\left(h\nu - E_g^T\right)^r \qquad (12)$$

According to the given equation, B is a constant and E_g^T is the Tauc energy gap, with the variable *r* being an index characterizing the absorption process. In a study of thin solid films of Fe(phen), it was found that *r = 2* for the direct band gap and *r = 1/2* for the indirect band gap. Plotting $(\alpha h\nu)^2$ against *hν* showed that the best fit was a linear relation given by equation (12), suggesting that the interband transition in Fe(phen) thin films is due to the indirect transition. The optical Tauc band gap for Fe(phen) thin films was obtained by plotting $(\alpha h\nu)^2$ against hν in Figure (6) and extrapolating the linear region of the plot where ($\alpha h\nu = 0$). The absorption coefficient is a measure of the material's ability to absorb light per unit length and is affected by various factors such as composition, structure, purity, and the wavelength of the incident light. Analyzing the absorption coefficient as a function of wavelength can provide information about the material's electronic and optical properties, including energy levels and band structure.

Absorption Coefficient: $\alpha = \frac{2.303*A}{l}$ (13)

Where: α: Absorption Coefficient, A: Absorbance, l: Thickness of thin film

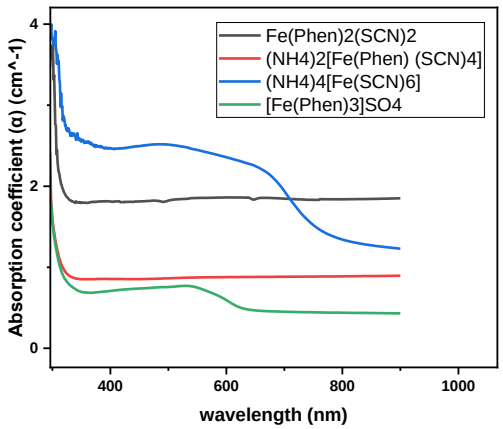

Figure 5: *The relationship between absorption coefficient (α) and wavelength for Fe(phen) thin films at thickness 100 nm.*

The absorption coefficient graph exhibits an atypical pattern, where absorption initially rises and then declines. This anomaly could be due to several factors, including the presence of impurities or defects within the material, surface roughness or scattering effects, or interference effects that arise from the interaction of light with the material's structure. To pinpoint the exact mechanisms accountable for this behaviour, additional analysis and characterization are necessary. In non-crystalline materials, defects could also be a factor.

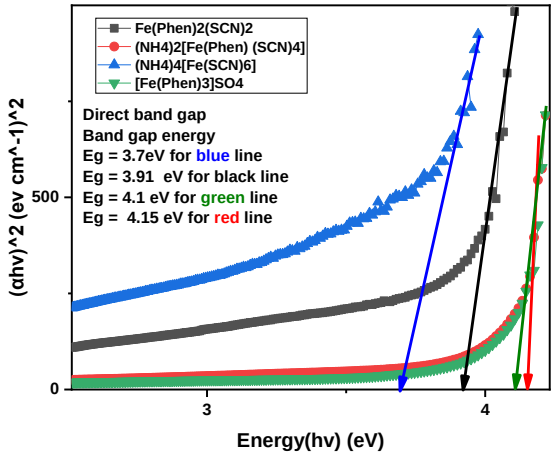

Figure 6: *The relationship between(αhv)²and photon energy for directFe (phen) thin films at thicknesses 100 nm*

The information provided suggests that the direct band gap graph is the most suitable method for extrapolating data on the x-axis shown in Figure 6. Analysis of the graph reveals that $Fe(phen)_2(SCN)_2$ has an energy gap value of 3.91eV, while $(NH_4)_4[Fe(SCN)_6]$, $(NH_4)_2[Fe(phen)(SCN)_4]$, and $[Fe(phen)_3]SO_4$ have energy gap values of 3.7 eV, 4.15eV and 4.1 eV, respectively. This indicates that $Fe(phen)_2(SCN)_2$, which contains Iron 1,10-phenanthroline molecular, has a smaller energy gap. However, it is important to acknowledge that other factors can impact the energy gap value. Therefore, when studying direct Fe(phen) thin films at a thickness of 100 nm, it is necessary to consider additional factors beyond the relationship between photon energy and constants depicted in the direct band gap graph. In summary, the topic revolves around examining the relationship between photon energy and constants for direct Fe(phen) thin films at a thickness of 100nm. The direct band gap graph is used for extrapolation on the x-axis, and the results highlight a smaller energy gap for $Fe(phen)_2(SCN)_2$, although other factors can also influence the energy gap value. The dielectric constant is a significant characteristic of optical materials, which are made up of both Real and Imaginary parts. It offers information about the permittivity and polarizability of a substance, which is related to the density of states within the forbidden energy gap.

The Real part of the dielectric constant indicates the extent to which the speed of light can be slowed down in the material, while the Imaginary part indicates the absorption of energy by an electric field due to dipole motion. To calculate both the real and imaginary parts of the dielectric constant from UV-visible absorption data:

$$\varepsilon_r = n^2 - k^2 \qquad (14)$$
$$\varepsilon_i = 2nk \qquad (15)$$

The formula for Urbach Energy (Eu), which is $\propto = \propto_\circ \mathbf{exp}\left(\frac{hv-Eg}{Eu}\right)$, can be rewritten as:

$$\boldsymbol{ln}\propto = \frac{1}{Eu}\boldsymbol{hv} - \frac{Eg}{Eu} + \boldsymbol{ln}\propto_\circ \qquad (16)$$

This equation is similar to the straight-line equation:

$$y = mx + c \qquad (17)$$

By comparing these two equations, we can see that the slope of the line in equation 16 is equal to one over the Urbach energy, the y-axis represents $\boldsymbol{ln}\propto$, and the x-axis represents $\boldsymbol{hv}$. The constant term in equation 16 corresponds to the y-intercept. Therefore, if we graph $\boldsymbol{ln}\propto$ on the y-axis and $\boldsymbol{hv}$ on the x-axis, the slope of the line will give us the inverse of the Urbach energy.

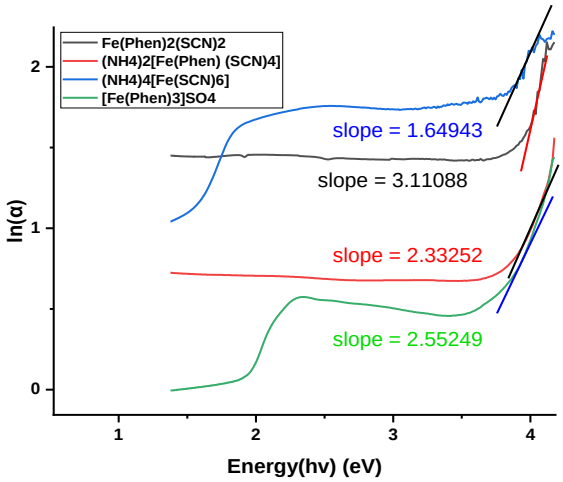

Figure 7: *The relationship between the ln(∝) and photon energy*

Now the slope of $(Fe(phen)_2(SCN)_2)$ comes out to be (3.11088). Put this value to get the $Urbach\ energy$ in eV. Thus, Urbach energy comes out to be (0.321 eV) or (321 meV) shown in Figure 7. And the slope of$((NH_4)_4[Fe(SCN)_6])$comes out to be (1.64943). Put this value to get the Urbach energy in eV. Thus, $Urbach\ energy$ comes out to be (0.606eV) or (606 meV). And the slope of $((NH_4)_2[Fe(phen)(SCN)_4])$ comes out to be (2.33252). Put this value to get the Urbach energy in eV. Thus, $Urbach\ energy$ comes out to be (0.428 eV) or (428 meV). And the slope of $([Fe(phen)_3]SO_4)$ comes out to be (2.55249). Put this value to get the Urbach energy in eV. Thus, $Urbach\ energy$ comes out to be (0.391eV) or (391 meV).

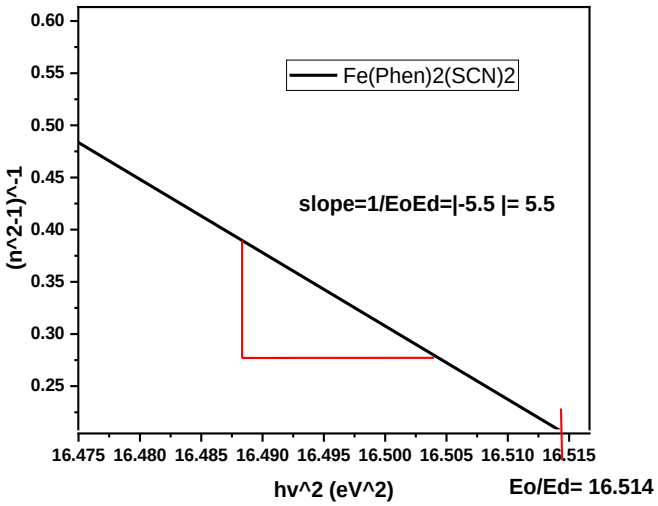

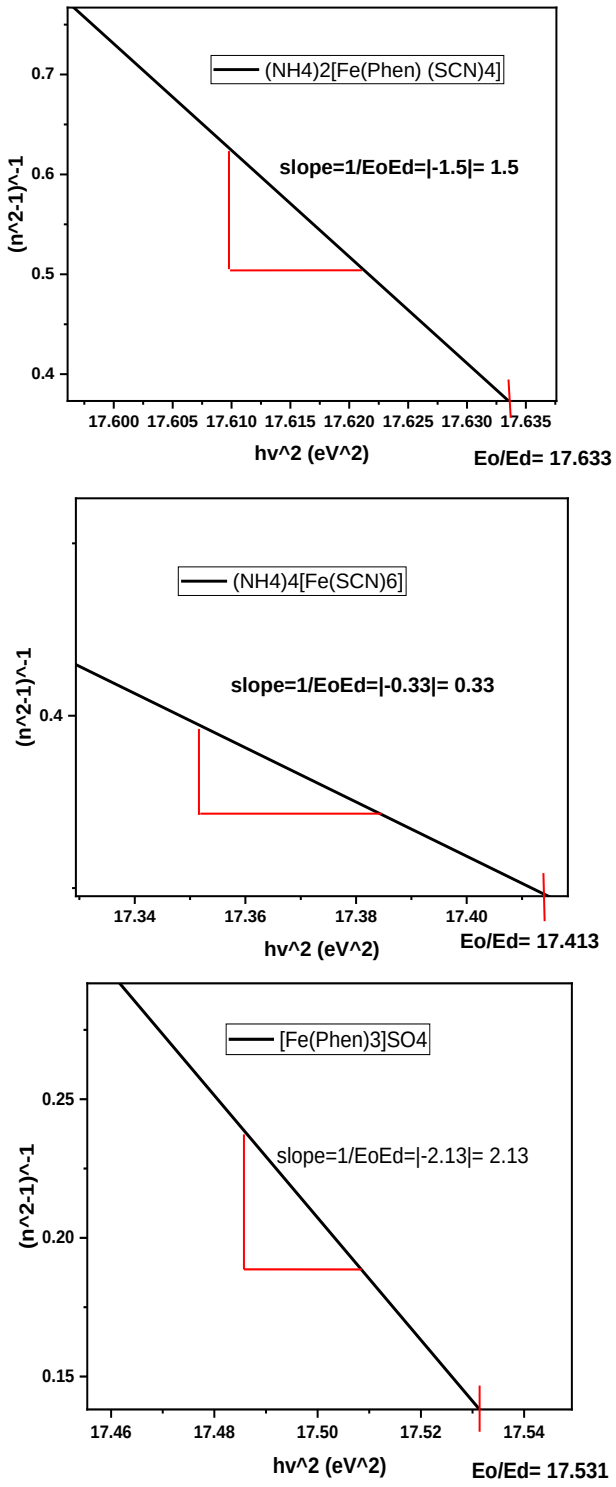

Figure 8: *The relationship between* $(hv)^2$ *and* $(n^2-1)^{-1}$

The Urbach energy is a parameter used to describe the width of the tail of the exponential absorption edge of a semiconductor material. It characterizes the degree of disorder and structural imperfections in the material, such as defects and impurities. When the Urbach energy decreases, it means that the tail of the absorption edge becomes narrower, indicating that the material has fewer structural imperfections and is more ordered. This can result in higher carrier mobility and improved optical properties, such as increased transparency and reduced absorption losses [19]. Band gap energy is the difference in energy between the valence band and the conduction band of a solid material.

Table 2:
The estimated values of the oscillator parameters of Fe (phen)thin films

Complexes	Oscillation Energy E_o(eV)	Dispersion Energy E_d(eV)	Field strength (f) $(eV)^2$	$n^2(o)$	ε_∞	M_1 (eV)	M_3 (eV)
$Fe(phen)_2(SCN)_2$	1.7338	0.1049	0.1818	1.06	1.029	0.06	0.02
$(NH_4)_2[Fe(phen)(SCN)_4]$	3.4163	0.1944	0.6641	1.057	1.028	0.056	0.005
$(NH_4)_4[Fe(SCN)_6]$	7.2541	0.4175	3.0285	1.057	1.028	0.057	0.001
$[Fe(phen)_3]SO_4$	2.8715	0.1637	0.47	1.057	1.028	0.039	0.0047

$E_g^{WWD} \approx E_o$

Table 3:
The calculated values of energy gap by Wemple-DiDomenico approximation, Tauc relation and calculated values of Urbach tails energy

Complexes	$E_g^{WWD}(eV)$	$E_g^T(eV)$	$E_u\,(meV)$
$Fe(phen)_2(SCN)_2$	1.7338	3.91	321
$(NH_4)_2[Fe(phen)(SCN)_4]$	3.4163	4.15	428
(NH4)4[Fe(SCN)6]	7.2541	3.7	606
$[Fe(phen)_3]SO_4$	2.8715	4.1	391

According to Figure 9, the peak values of susceptibilities ($\chi^{(3)}$) are$1.67 * 10^{-15}$ surf $(Fe(phen)_2(SCN)_2)$,$7.17 * 10^{-15}$ surf $(NH_4)_2[Fe(phen)(SCN)_4]$,$3.25 * 10^{-7}$ esu of $(NH_4)_4[Fe(SCN)_6]$ and $7.05 * 10^{-15}$ esuof $[Fe(phen)_3]SO_4$). The figure illustrates the relationship between the third-order nonlinear optical susceptibility and photon energy. Experimental data demonstrates that various materials exhibit distinct peak values of susceptibility. The figure also indicates that the susceptibility increases as photon energy increases, likely due to an increase in the number of excited electrons and the given energy value of 2.525 eV for $Fe(phen)_2(SCN)_2$ allows us to calculate the corresponding wavelength using the equation λ = hc/E. Hence, the calculated wavelength is approximately 491.4 nm. Similarly, for $(NH_4)_2[Fe(phen)(SCN)_4]$ with an energy of 3.25 eV, the wavelength is approximately 381.6 nm. In the case of $(NH_4)_4[Fe(SCN)_6]$ with an energy of 1.97 eV, the wavelength is approximately 629 nm. Lastly, for $[Fe(phen)_3]SO_4$) with an energy of 2.345 eV, the wavelength is approximately 529.5 nm as

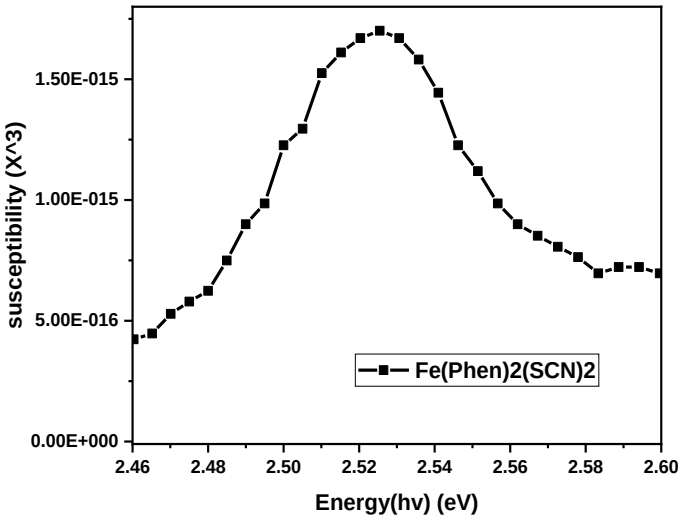

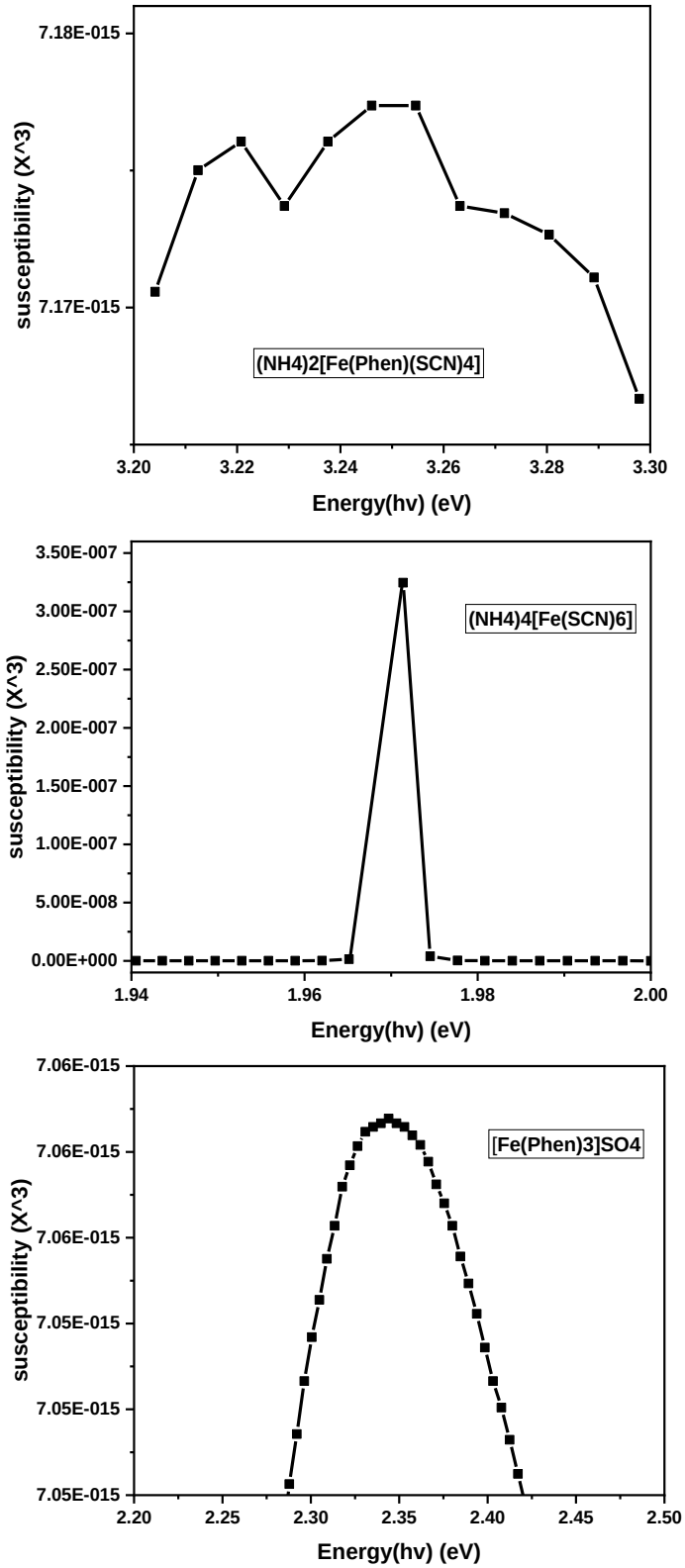

Figure 9: *The relationship of the third order nonlinear optical susceptibility and photon energy*

4. Nonlinear Optical Properties in Spin Crossover (SCO) Compounds

The third-order nonlinear optical susceptibility ($\chi^{(3)}$) describes the response of a material to an intense electromagnetic field, and it is related to the electronic properties of the material. $Iron\ (phen)$ is a complex that exhibits spin transition, which is the switching of the iron ion between two states with different spin configurations .The spin transition in $iron\ (phen)$ alters the electronic structure of the complex and can lead to changes in the energy levels of the electrons. These changes, in turn, can affect the $\chi^{(3)}$ value of the complex [21][22]. In the low-spin (LS) state, the electronic structure of the $iron\ (phen)$ complex is relatively simple, with only a few electronic transitions contributing to the nonlinear response. However, in the high-spin (HS) state, the electronic structure becomes more complex, with many additional electronic transitions contributing to the $\chi^{(3)}$ value [23]. As a result, the spin transition in $iron\ (phen)$ can lead to a significant increase in the $\chi^{(3)}$ value of the complex. This effect has been observed in experiments, where the $\chi^{(3)}$ value of iron (phen) was found to increase by several orders of magnitude when the iron ion underwent a spin transition. Finally, the spin transition in $iron\ (phen)$ can alter the electronic properties of the complex and, in turn, affect its $\chi^{(3)}$ value. This effect is due to changes in the energy levels of the electrons and the number of electronic transitions contributing to the nonlinear response [24].

5. Conclusion

Iron 1,10-phenanthroline molecular nanolayers were synthesized using complexation reactions method. Fe^{2+}(Phen) molecular thin films were then prepared from these nanolayers as samples. The prepared thin films were subjected to characterization using XRD and UV-Vis spectroscopy to investigate their optical properties, thickness of the thin film was measured with a profile meter, and absorbance, transmittance, and reflectivity were measured by $UV-Vis$ spectrophotometer. Four iron ionat thicknesses (100 nm) were measured. The single oscillator model governs the dispersion of the refractive index in the film, the oscillator parameters were determined using this approach, and the direct energy gap (E_g^{WDD}) was computed using the $Wemple-DiDomenico$ approximation, and the third order nonlinear optical susceptibility ($\chi^{(3)}$) was measured using Miller's formula. The optical band is studied using the absorption spectrum, and the direct energy gap was computed using several approaches such as Tauc's relation (E_g^T), Absorption, localized tail states, the concepts of Urbach energy (Eu) and bandgap were thoroughly discussed, and the Urbach energy (Eu) value was obtained by calculating the gradient, as illustrated in Figure 7.The computed values of the energy gap using the various methodologies indicated in Table 3 that the $Fe(phen)_2(SCN)_2$ has a smaller energy gap compared with other molecules. The value of nonlinear optical susceptibility ($\chi^{(3)}$) suggested that the novel polymer might be widely utilized in a variety of photonic electronic applications. As for the optical absorption coefficient, it was found that it increases rapidly with increasing photon energy, which gives a clear indication of the possibility of using it in the fields of commercial optical communications and electronic industry fields such as electrical circuits that it is used in modern devices such as electronic calculators, electron microscopes, electrical switches, and optical imaging. The spin transition in $iron\ (phen)$ can alter the electronic properties of the complex and, in turn, affect its $\chi^{(3)}$ value. This effect is due to changes in the energy levels of the

electrons and the number of electronic transitions contributing to the nonlinear response.

Data availability statement: The whole data of this research is included in this article.

Declaration of competing interest: The authors declare that they have no known competing financial interests or personal relationships that could have appeared to influence the work reported in this paper.

References

1. A. Bencini and V. Lippolis, "1, 10-Phenanthroline: A versatile building block for the construction of ligands for various purposes," *Coord. Chem. Rev.*, vol. 254, no. 17–18, pp. 2096–2180, 2010.
2. J.-F. Létard, P. Guionneau, and L. Goux-Capes, "Towards spin crossover applications," in *Spin Crossover in Transition Metal Compounds III*, 2004.
3. J. E. Monat and J. K. McCusker, "Femtosecond excited-state dynamics of an iron (II) polypyridyl solar cell sensitizer model," *J. Am. Chem. Soc.*, vol. 122, no. 17, pp. 4092–4097, 2000.
4. A. Hauser, "Ligand field theoretical considerations," *Spin Crossover Transit. Met. Compd. I*, pp. 49–58, 2004.
5. P. Gütlich, H. A. Goodwin, and Y. Garcia, *Spin crossover in transition metal compounds I*, vol. 1. Springer Science \& Business Media, 2004.
6. S. Decurtins, P. Gütlich, C. P. Köhler, H. Spiering, and A. Hauser, "Light-induced excited spin state trapping in a transition-metal complex: The hexa-1-propyltetrazole-iron (II) tetrafluoroborate spin-crossover system," *Chem. Phys. Lett.*, vol. 105, no. 1, pp. 1–4, 1984, doi: 10.1016/0009-2614(84)80403-0.
7. A. Hauser, "Intersystem crossing in the [Fe (ptz) 6](BF4) 2 spin crossover system (ptz= 1-propyltetrazole)," *J. Chem. Phys.*, vol. 94, no. 4, pp. 2741–2748, 1991.
8. J. J. McGravey and I. Lawthers, "Photochemically-induced perturbation of the 1 A⇌ 5 T equilibrium in Fe 11 complexes by pulsed laser irradiation in the metal-to-ligand charge-transfer absorption band," *J. Chem. Soc. Chem. Commun.*, no. 16, pp. 906–907, 1982.
9. H. T. Lemke *et al*., "Coherent structural trapping through wave packet dispersion during photoinduced spin state switching," *Nat. Commun.*, vol. 8, no. 1, p. 15342, 2017.
10. C. Bressler *et al*., "Femtosecond XANES study of the light-induced spin crossover dynamics in an iron (II) complex," *Science (80-.).*, vol. 323, no. 5913, pp. 489–492, 2009.
11. A. Al-Hilo *et al*., "2-D and mott transition studies on metal (M) doped PrBa2Cu 3O7," *J. Low Temp. Phys.*, vol. 173, no. 3–4, pp. 89–105, 2013, doi: 10.1007/s10909-013-0893-7.
12. F. A. Kasim, M. A. Mahdi, J. J. Hassan, and S. J. Kasim, "Preparation and optical properties of CdS / Epoxy nanocomposites," vol. 5, pp. 57–66, 2012.
13. W. C. Tan, K. Koughia, J. Singh, and S. O. Kasap, "Fundamental optical properties of materials I," *Opt. Prop. Condens. matter Appl.*, vol. 6, p. 1, 2006.
14. J. I. Pankove, *Optical processes in semiconductors*. Courier Corporation, 1975.
15. H. \cSAFAK, M. Merdan, and Ö. F. Yüksel, "Dispersion analysis of SnS and SnSe," *Turkish J. Phys.*, vol. 26, no. 5, pp. 341–348, 2002.
16. H. M. Jabbar, "Optical Properties of vanadium pentoxide prepared by sol gel method," *J. Kufa-Physics*, vol. 10, no. 01, 2018.
17. S. Il\ican, M. Zor, Y. Ça\uglar, and M. Ça\uglar, "Optical characterization of the CdZn (S1-xSex)(2) thin films deposited by spray pyrolysis method," 2006.
18. H. Fujiwara, *Spectroscopic ellipsometry: principles and applications*. John Wiley \& Sons, 2007.
19. H. M. Jabbar, E. M. Jaboori, and A. Q. Abdullah, "Dispersion parameters, optical constant and photoluminescence of poly vinyl alcohol grafted eosin-Y dye (PVA-g-Ei)," *J. Basrah Res.(Sci.)*, vol. 36, pp. 9–16, 2010.
20. H. B. Tarikhum, F. Almyahi, and B. Ali, "Optical, Structural, and Electrochemical Properties of P3HT:Y6 Photoactive Layer for Organic Photovoltaics," *Karbala Int. J. Mod. Sci.*, vol. 9, no. 4, pp. 618–627, 2023, doi: 10.33640/2405-609X.3328.
21. C. R. Nayar and R. Ravikumar, "Second order nonlinearities of Schiff bases derived from salicylaldehyde and their metal complexes," *J. Coord. Chem.*, vol. 67, no. 1, pp. 1–16, 2014.
22. T. Yang, M. Kurmoo, and M.-H. Zeng, "Recent advances of single-crystal to single-crystal transformation for discrete coordination compounds," *J. Indian Inst. Sci.*, vol. 97, pp. 299–309, 2017.
23. H. A. Badran, A. A. Al-Fregi, R. K. F. Alfahed, and A. S. Al-Asadi, "Study of thermal lens technique and third-order nonlinear susceptibility of PMMA base containing 5′, 5″-dibromo-o-cresolsulfophthalein," *J. Mater. Sci. Mater. Electron.*, vol. 28, pp. 17288–17296, 2017.
24. D. N. Christodoulides, I. C. Khoo, G. J. Salamo, G. I. Stegeman, and E. W. Van Stryland, "Nonlinear refraction and absorption: mechanisms and magnitudes," *Adv. Opt. Photonics*, vol. 2, no. 1, pp. 60–200, 2010.

Journal of Engineering, Science and Technological Trends (JESTT)
Vol. 1, Issue 2, August 2024
DOI: https://doi.org/10.48112/jestt.v1i2c.2

Article

Mega Hydropower Projects and Sustainable Development of Pakistan

Muhammad Adeel Afzal[1], Jamil Afzal[2*] and Zuhaib Nishtar[3]

[1]College of Economics & Management Science, China Three Gorges University, Yichang, China

[2]Faculty of Law and Political Sciences, Islamic Azad University, Tehran, Iran

[3]Department of Electrical Engineering and New Energy, China Three Gorges University, China

* Corresponding Email: sirjamilafzal@gmail.com (J. Afzal)

Received: 19 December 2023 / Revised: 24 August 2024 / Accepted: 26 August 2024 / Published Online: 31 August 2024

ABSTRACT

This research paper aims to contribute to discussing the impact of mega hydro projects on sustainable development in Pakistan. It is essential to carefully consider the long-term impact of these projects on social, economic, and environmental factors to ensure that they contribute to sustainable development and the population's well-being. Data was collected through a combination of primary and secondary sources; primary sources were field observations, while secondary sources were government reports, academic articles, and other relevant literature. While the project has the potential to generate clean energy and contribute to economic development, it also has negative impacts on the environment and local communities. To contribute to sustainable development of Pakistan, while minimizing its potential negative impact on the environment, social well-being, and economic growth of the region. The study recommendations aim to ensure that the Sukhi Kinari Dam contributes to sustainable development in Pakistan while minimizing its potential negative impact on the environment, social well-being, and economic growth of the region.

Keywords: Sukhi Kinari Dam; Mega Hydropower Project; Policy Framework; Sustainable Development

1. Introduction

Pakistan is a developing country that faces a growing demand for energy, economic development, and infrastructure [1]. In this context, mega hydro projects such as the Sukhi Kinari Dam have been proposed as a solution to these challenges. However, it is important to examine the potential impact of such projects on sustainable development in the country [2]. Sustainable development [3] seeks to address the current needs while ensuring that future generations can fulfill their requirements without compromise. Therefore, it's necessary to consider the long-term social, economic, and environmental impact of these projects [4].

The purpose of this research paper is to examine the impact of the Sukhi Kinari Dam on sustainable development in Pakistan. The paper provided an overview of sustainable development and its goals, as well as a literature review of previous research on the impact of hydroelectric projects on sustainable development. The paper also includes a methodology section outlining the research design and data analysis techniques used to collect and analyze data on the Sukhi Kinari Dam project. The findings of the research paper will provide insight into the impact of the Sukhi Kinari Dam project on sustainable development in Pakistan. The paper discussed the positive impacts of the project, such as energy generation, economic growth, the generation of jobs, and the adverse effects, such as those on the environment and society.

2. Literature Review

A definition of sustainable development is that it involves achieving present needs while safeguarding the capability of future generations to fulfill their requirements [5]. Hydroelectric projects are often proposed as a solution to the growing demand for energy, economic development, and infrastructure in developing countries like Pakistan [6]. However, the potential impact of these projects on sustainable development is a topic of debate among scholars and policymakers. Earlier studies have demonstrated that hydroelectric projects can bring about both favourable and adverse effects on the sustainability of development. On the positive side, hydroelectric projects can generate clean energy, reduce reliance on fossil fuels, and provide economic benefits such as job creation and increased revenue for the government [7]. For example, a study by Mazhar et al. [8] found that the Tarbela Dam, another hydroelectric project in

Pakistan, contributed significantly to economic development and poverty reduction in the area. However, hydroelectric projects can also have negative impacts on sustainable development. For example, the construction of dams can displace local communities, destroy wildlife habitats, and alter the natural flow of rivers, which can have downstream ecological impacts. Additionally, the operation of dams can lead to changes in water quality and quantity, which can affect the livelihoods of people who depend on the river for irrigation or fishing. A study by Afzal et al. [9] found that the construction of the Gomal Zam Dam in Pakistan had negative impacts on the environment and local communities. The Sukhi Kinari Dam, a mega hydro project under construction in Pakistan, is expected to have a significant impact on sustainable development in the country. Previous research on the project has focused on its potential impact on energy generation and economic development. For example, a study by Khan et al. [10] found that the project could generate significant energy and contribute to economic development in the region. However, there is limited research on the potential negative impacts of the Sukhi Kinari Dam project on sustainable development, particularly on environmental and social factors [11]. Therefore, further research is needed to understand the potential trade-offs between the positive and negative impacts of the project on sustainable development in Pakistan. This research paper aims to contribute to this discussion by examining the impact of the Sukhi Kinari Dam on sustainable development in Pakistan, with a focus on its environmental and social impacts.

3. Methodology

The impact of a Mega hydro project on sustainable development in Pakistan can be accessed through a case study of the Sukhi Kinari Dam. A comprehensive literature review of existing research and literature on the topic of Mega hydro projects and sustainable development in Pakistan was conducted. It provides a foundation for the study and helps identify gaps in knowledge that the study addressed. Data was collected through a combination of primary and secondary sources using a mixed method of study [12]. Primary sources were field observations, while secondary sources were government reports, academic articles, and other relevant literature.

3.1. Data Collection

Data was collected on the following aspects:

Environmental impact: The impact of the Sukhi Kinari Dam on the environment was assessed; it includes the impact on the local ecology, water quality, and air quality.

***Social impact*:** The social impact of the dam was assessed; it included the impact on local communities, including their livelihoods and access to resources.

***Economic impact*:** The economic impact of the dam was assessed; it includes the impact on the local economy, including job creation and income generation.

***Infrastructure and technology*:** The infrastructure and technology used in the construction and operation of the dam were assessed, including its safety and sustainability.

3.2. Data Analysis

The data was gathered and underwent scrutiny through suitable quantitative and qualitative techniques, encompassing statistical analysis, content analysis, and thematic analysis. The study's conclusions, which include the advantages and disadvantages of the Sukhi Kinari Dam for Pakistan's sustainable development, were addressed and presented. Based on the findings of the study, conclusions were drawn and recommendations were made for improving the sustainability of Mega hydro projects in Pakistan. Overall, this methodology provided a comprehensive assessment of the impact of Mega hydro projects on sustainable development in Pakistan, using the Sukhi Kinari Dam as a case study.

4. Regulatory and Policy Framework

The regulatory and policy framework for mega hydro projects in Pakistan is complex and involves several key institutions and legal frameworks. The regulatory framework is intended to ensure that mega hydro projects are developed in a way that promotes sustainable development and protects the environment, social well-being, and economic growth of the country. One of the key regulatory institutions for mega hydro projects in Pakistan is the Water and Power Development Authority (WAPDA) [13]. WAPDA is responsible for the planning, design, construction, and operation of hydroelectric power projects in Pakistan. WAPDA is also responsible for ensuring that mega hydro projects comply with relevant laws and regulations, including the Pakistan Environmental Protection Act 1997 [14]. The Pakistan Environmental Protection Agency (EPA) is another key regulatory institution for mega hydro projects in Pakistan. The EPA is responsible for reviewing and approving environmental impact assessments (EIAs) for mega hydro projects. The EPA is also responsible for monitoring compliance with environmental regulations and taking enforcement action when necessary[15].

In addition to these institutions, several key legal frameworks govern mega hydro projects in Pakistan. The Pakistan Environmental Protection Act 1997 sets out the legal requirements for environmental impact assessments and environmental protection in Pakistan [16, 17]. The National Energy Policy 2013 provides a policy framework for the development of renewable energy, including hydroelectric power, in Pakistan [18]. Several international agreements and standards govern mega hydro projects in Pakistan. These include the World Commission on Dams Guidelines on Dam Safety and the United Nations Framework Convention on Climate Change [19].

Despite the existence of these regulatory and policy frameworks; there have been concerns about their effectiveness in ensuring environmental, social, and economic sustainability in mega hydro projects in Pakistan. For example, there have been concerns about the adequacy of environmental impact assessments for mega hydro projects, and about the displacement of local communities and the impact on downstream water supply. The regulatory and policy framework for mega hydro projects in Pakistan involves several key institutions and legal frameworks. While these frameworks are intended to ensure sustainable development and protect the environment, social well-being, and economic growth of the country, there have been concerns about their effectiveness in practice. To ensure that mega hydro projects like the Sukhi Kinari Dam contribute to sustainable development in Pakistan, it is important to monitor and evaluate the implementation of these regulatory and policy frameworks and make improvements as necessary.

5. Finding

The development findings of the impact of the Sukhi Kinari Dam on sustainable development in Pakistan are mixed. While the project has the potential to generate clean energy and contribute to economic development, it also has negative impacts on the environment and local communities. On the positive side, the Sukhi Kinari Dam is expected to generate 884 MW of clean energy, which can help reduce Pakistan's reliance on fossil fuels and mitigate the impacts of climate change [20]. The project is also

expected to create jobs and contribute to economic development in the region, particularly in the construction and operation of the dam. However, the Sukhi Kinari Dam also has negative impacts on the environment and local communities. The construction of the dam has already resulted in the displacement of some people, who were relocated to nearby areas. This has disrupted their traditional way of life and livelihoods, and they may face challenges in accessing basic services like healthcare and education. The dam has also caused the loss of forest land and is expected to impact the biodiversity of the area. Furthermore, the operation of the dam can have negative impacts on downstream communities and the river ecosystem. The dam will alter the natural flow of the Kunhar River, which may affect the water quality and quantity downstream, impacting the livelihoods of people who depend on the river for irrigation and fishing.

To mitigate these negative impacts, it is important to implement measures that promote sustainable development. For example, compensation and resettlement programs can be implemented to ensure that affected communities are adequately compensated and can access basic services. Environmental safeguards and monitoring systems [21] can be put in place to minimize the impact on biodiversity and the ecosystem. Additionally, community-based approaches can be used to ensure that local communities are involved in decision-making processes and can benefit from the project. The Sukhi Kinari Dam has the potential to contribute to sustainable development in Pakistan by generating clean energy and contributing to economic development. However, the negative impacts of the project on the environment and local communities cannot be ignored. It is important to implement measures to mitigate [22] these impacts and ensure that the project contributes to sustainable development in the long term.

6. Recommendations

Based on the analysis of the impact of the Sukhi Kinari Dam on sustainable development in Pakistan, the following recommendations are suggested:

- The project developers should take measures to minimize the environmental impact of the dam, including minimizing the loss of biodiversity, reducing greenhouse gas emissions, and preventing soil erosion. The implementation of these measures should be monitored regularly to ensure their effectiveness.
- A comprehensive social impact assessment should be conducted to evaluate the potential impact of the dam on local communities, including the impact on their livelihoods, cultural heritage, and social structures. The assessment should be conducted in a participatory manner, involving local communities and stakeholders.
- The project developers should engage with local communities and stakeholders throughout the project lifecycle, to ensure that their concerns and interests are taken into account. This should include providing information [23] about the project, consulting with local communities, and ensuring their participation in decision-making processes.
- Adequate compensation and resettlement should be provided to those affected by the project, including those displaced from their homes or livelihoods. The compensation should be fair and transparent, and based on a comprehensive assessment of the impact of the project on affected individuals and communities.
- The project developers should prioritize the employment of local people in the construction and operation of the dam, and provide training and capacity-building opportunities to local communities to enable them to participate in the project's development and management.
- The government of Pakistan should also invest in the development of alternative energy sources, such as solar and wind energy.

7. Conclusion

The impact of the Mega Hydropower Project on the sustainable development of Pakistan is a subject of paramount importance and complexity. Our comprehensive analysis, employing a range of qualitative methods, has unveiled a nuanced picture of a colossal endeavor. The project offers substantial potential for economic growth, job creation, and meeting the country's energy needs. It can pave the way for reduced reliance on fossil fuels and contribute to a more sustainable energy mix. However, this potential must be carefully managed to ensure that it doesn't come at the cost of significant environmental degradation or adverse social consequences. The recommendations above aim to ensure that the Sukhi Kinari Dam contributes to sustainable development in Pakistan while minimizing its potential negative impact on the environment, social well-being, and economic growth of the region. Implementation of these recommendations will require collaboration between project developers, government institutions, local communities, and other stakeholders, with transparency, participation, and accountability.

Data availability statement: The whole data of this research is included in this article.

Declaration of competing interest: The authors declare that they have no known competing financial interests or personal relationships that could have appeared to influence the work reported in this paper.

References

1. Xu, Z., et al., *China-Pakistan Cultural Exchanges and Cooperation under Belt & Road Initiative*. Siazga Research Journal, 2023. **2**(3).
2. Qayum, M., J. Afzal, and M. Qayyum, *ROLE OF WOMEN IN SUSTAINABLE DEVELOPMENT IN PAKISTAN: THE POST DEVELOPMENT GOAL*.
3. Afzal, J., et al., *Sustainable Development and Integrity of Fishery Sector in Pakistan.* Siazga Research Journal, 2023. **2**(3).
4. Afzal, J., et al., *A Fundamental Study on the Psychological Impact of Global Climate Change.* Technology (WD-EST'23), 2023. **3**: p. 05.
5. Emas, R., *The concept of sustainable development: definition and defining principles.* Brief for GSDR, 2015. **2015**: p. 10-13140.
6. Nishtar, Z. and J. Afzal, *History of emerging trends of renewable energy for sustainable development in Pakistan.* Journal of History and Social Sciences, 2023. **14**(1): p. 126-139.
7. Afzal, J. and Z. Nishtar, *A Substantial Study on History of Climate Change in South Asia for Sustainable Development.* Journal of History and Social Sciences, 2023. **14**(1): p. 101-112.
8. Mazhar, N., et al., *Effects of climatic factors on the sedimentation trends of Tarbela Reservoir, Pakistan.* SN Applied Sciences, 2021. **3**: p. 1-9.
9. Afzal, J., et al., *Effects of dam on temperature, humidity and precipitation of surrounding area: a case study of Gomal Zam Dam in Pakistan.* Environmental Science and Pollution Research, 2023. **30**(6): p. 14592-14603.
10. Khan, I., L. Han, and H. Khan, *Renewable energy consumption and local environmental effects for economic growth and carbon emission: evidence from global income countries.* Environmental Science and Pollution Research, 2021: p. 1-18.
11. Gul, E., *Reaping socio-economic blessings of flowing water: evidence from hydropower initiatives of China-Pakistan Economic Corridor*. International Journal of Water, 2018. **12**(4): p. 314-341.
12. Yongmei, C. and J. Afzal, *Impact of Enactment of 'The Prevention of Electronic Crimes Act, 2016'as Legal Support in Pakistan.* Academy of Education and Social Sciences Review, 2023. **3**(2): p. 203-212.
13. Khan, M.Y.A., et al. *Cost Benefit Based Analytical Study of Automatic Meter Reading (AMR) and Blind Meter Reading (BMR)*

used by PESCO (WAPDA). in *2020 3rd International Conference on Computing, Mathematics and Engineering Technologies (iCoMET)*. 2020. IEEE.
14. Adam, A., S. Mukhtar, and A. Amir, *An Analysis of Environmental Crisis under Environmental Constitutionalism in Pakistan.* Islamabad Law Review, 2022. **6**(2): p. 22-42.
15. Khan, M., et al., *Performance of EIA authority and effectiveness of EIA system in Pakistan.* Environmental Impact Assessment Review, 2020. **81**: p. 106357.
16. Sial, S.A., S.M.A. Zaidi, and S. Taimour, *Review of existing environmental laws and regulations in Pakistan*. 2018: WWF-Pakistan Punjab, Pakistan.
17. Ilyas, M., et al., *Environmental and health impacts of industrial wastewater effluents in Pakistan: a review*. Reviews on environmental health, 2019. **34**(2): p. 171-186.
18. Irfan, M., et al., *SWOT analysis of energy policy 2013 of Pakistan.* European Journal of Engineering Science and Technology, 2019. **2**(1): p. 71-94.
19. Baghel, R. and M. Nüsser, *Discussing large dams in Asia after the World Commission on Dams: Is a political ecology approach the way forward?* Water alternatives, 2010. **3**(2).
20. Baloch, M.H., et al., *Hybrid energy sources status of Pakistan: An optimal technical proposal to solve the power crises issues.* Energy Strategy Reviews, 2019. **24**: p. 132-153.
21. Yihong, Z. and J. Afzal, *An IoT-Based Mechanism for Monitoring Dam Structures*. 2023, EasyChair.
22. Afzal, J. and M. Qayyum, *An Analysis of Risks, Obstacles and Mitigation Impoverishment in Development: Induced Displacement and Resettlement.* Siazga Research Journal, 2023. **2**(2): p. 101-109.
23. Afzal, J. and C. Yongmei, *Federal and provincial legislation regarding 'Right to Information'for good governance in Pakistan.* Discover Global Society, 2023. **1**(1): p. 12.

Journal of Engineering, Science and Technological Trends (JESTT)
Vol. 1, Issue 2, August 2024
DOI: https://doi.org/10.48112/jestt.v1i2c.3

Review

A Short Review Note on Finite Element Method for Hydraulic Structural Engineering

Soraya Sarwari[1*], Yan Qiao[1] and Muhammad Abubakar Rafi[2]

[1]College of Hydraulic & Environmental Engineering, China Three Gorges University, China

[2]Department of Physics, University of Agriculture Faisalabad, Pakistan

* Corresponding Email: sarwarisoraya24@gmail.com (S. Sarwari)

Received: 02 July 2024 / Revised: 23 August 2024 / Accepted: 26 August 2024 / Published Online: 31 August 2024

ABSTRACT

Dams play a critical role in water resources engineering, providing irrigation and drinking water through the creation of reservoirs. However, geotechnical and hydraulic engineers face challenges such as the possibility of piping events and collapse due to water leaking under the dam body, as well as variation in bearing capacity, void ratio, and water content in different regions of the ground where the dam body consolidates. The paper also highlights the advances in hydraulic structural engineering through the Finite Element Method (FEM) and other numerical modelling techniques, which have enabled more accurate design and analysis of hydraulic structures such as dams, spillways, weirs, and sluice gates. The maintenance and rehabilitation of these structures are also discussed, with a focus on developing non-destructive testing methods and innovative repair and retrofitting techniques to improve their structural integrity and hydraulic efficiency. The challenges and opportunities in hydraulic structural engineering research are explored, including the impact of climate change, sustainable design, and integration of new technologies like artificial intelligence and the Internet of Things. As hydraulic structures become more resilient and adaptive to withstand extreme events and support sustainable development, there will be an increased need for continued research and innovation in FEM and other advanced numerical modelling techniques to support hydraulic structural engineering advancements.

Keywords: Finite Element Method; Hydraulic Structures; Numerical Modeling; Sustainability

1. Introduction

Hydraulic structures are crucial infrastructural components for water resources management, providing various functions such as storage, conveyance, diversion, and regulation [1]. Hydraulic structural engineering is a multidisciplinary field that deals with the design, construction, maintenance, and management of these structures [2],[3]. The hydraulic structures include dams, weirs, barrages, spillways, channels, culverts, and other components that form an integral part of water supply systems [4].

Hydraulic structures often experience complex interactions with flowing water [5]. FEM allows the simulation of fluid-structure interaction problems where the movement of the water affects the structural response [6]. For instance, in the design of spillways or overflow structures, engineers must consider the impact of water forces on the structure, which FEM can model by coupling fluid dynamics with structural analysis. This is particularly critical in assessing [7] the performance of structures under extreme storm events or seismic activity [8]. In scenarios where hydraulic structures are built on or near soil, understanding the soil-structure interaction is vital. FEM can model the interaction between the structure and surrounding soil, accounting for factors such as soil consolidation, water table fluctuations, and pore pressure effects [9],[10]. This is important for structures like levees and embankments, where the stability and deformation of the soil can significantly influence structural performance. Utilizing FEM, engineers can perform sensitivity analysis and optimization of hydraulic structures [11]. By modelling different design variables such as material properties, geometric configurations, and reinforcement strategies, FEM enables engineers to identify the most efficient configurations that meet safety and performance requirements without extensive physical prototypes [12],[13]. Research progress in hydraulic structural engineering has been driven by the need for efficient, safe, and sustainable water resource management [14],[15]. The advances in this field are aimed at improving the performance and resilience of hydraulic structures, reducing their environmental impact, and ensuring their

long-term sustainability [16],[17]. This research progress has been achieved through a combination of experimental, numerical, and analytical techniques that have advanced our understanding of hydraulic behaviour, materials science, and structural mechanics[18],[19].

This review paper aims to provide a summary of the recent research progress in hydraulic structural engineering. The following are the objectives of this summary manuscript;

1 The paper will review the advances in the construction, maintenance, and management of hydraulic structures.
2 It will also highlight the challenges and opportunities in this field and suggest future research directions.
3 The paper will draw upon the latest research articles, technical reports, and conference proceedings to provide a comprehensive understanding of the research progress in hydraulic structural engineering.

2. Advancement in Hydraulic Engineering

Advances in the design of hydraulic structures have been made in recent years, the new technologies and improved understanding of the behaviour of these structures. Here are some of the key advances in hydraulic structure design:

The use of advanced materials, such as fibre-reinforced composites and high-performance concrete, has enabled engineers to design hydraulic structures that are more durable, resistant to corrosion, and have a longer service life [20]. Computational modelling, such as Finite Element Method (FEM) and Computational Fluid Dynamics (CFD), has made it possible for engineers to optimize the design of hydraulic structures by simulating their behaviour under different loading conditions [21]. 3D printing has enabled engineers to quickly and cost-effectively produce prototypes of hydraulic structures, allowing them to test and refine their designs before committing to large-scale production [22]. Innovative design approaches, such as biomimicry, have inspired engineers to design hydraulic structures that mimic the behaviour of natural systems, such as the flow of water in a river or the structure of a coral reef [23].

The use of sensors and other technologies to create smart structures has enabled engineers to design hydraulic structures that can monitor their health and detect potential failures before they occur [19],[24]. Overall, advances in the design of hydraulic structures have enabled engineers to create structures that are more durable, cost-effective, and sustainable, while also improving the safety and functionality of these critical infrastructure assets.

3. Numerical Analysis in Hydraulic Engineering

One of the techniques used in hydraulic structural engineering research is numerical modelling. Numerical modelling is a computational approach that allows engineers to simulate and predict the behaviour of hydraulic structures under different loading conditions [25],[26]. This technique involves the use of mathematical models and computer programs to solve complex equations and simulate the behaviour of hydraulic structures in a virtual environment [21],[27],[28].

Numerical modelling techniques have become increasingly sophisticated and powerful over the years, allowing for more accurate and reliable predictions of the behaviour of hydraulic structures [29]. Some of the commonly used numerical modelling techniques in hydraulic structural engineering research are:

FEM is a numerical technique that divides a complex structure into smaller elements and solves the equations governing the behaviour of each element. FEM is widely used for analyzing the stress, strain, and deformation of hydraulic structures under different loading conditions [30]. CFD is a numerical technique that simulates the flow of fluids in a hydraulic structure. CFD can be used to predict the velocity, pressure, and turbulence of fluid flow in a hydraulic structure, which is essential for designing and optimizing hydraulic structures [31]. DEM is a numerical technique that simulates the behaviour of granular materials, such as sediment and soil, in a hydraulic structure. DEM can be used to predict the movement and settling of sediment in a reservoir or river, which is important for managing sedimentation in hydraulic structures[32]. BEM is a numerical technique that solves equations at the boundary of a hydraulic structure. BEM is commonly used for simulating the behaviour of wave propagation and erosion in hydraulic structures [33].

Numerical modelling techniques have several advantages over traditional experimental methods in hydraulic structural engineering research. They are cost-effective, time-efficient, and allow for a more detailed analysis of complex hydraulic structures [34]. Numerical modelling techniques also provide a safe and controlled environment for testing and optimizing hydraulic structures, without the risk of physical damage or failure [35]. However, numerical modelling techniques also have limitations and challenges. The accuracy of numerical models depends on the quality and reliability of the input data, and uncertainties in the behaviour of hydraulic structures can affect the accuracy of the simulation results [36]. Therefore, numerical modelling techniques should be used in conjunction with experimental methods and field observations to ensure a comprehensive and reliable analysis of hydraulic structures.

3.1. Computational Fluid Dynamics (CFD)

Computational Fluid Dynamics (CFD) is a numerical modelling technique used to simulate the behaviour of fluids, such as water, in hydraulic structures. The technique involves solving a set of mathematical equations that describe the behaviour of fluid flow, such as velocity, pressure, and turbulence. To use CFD, engineers first create a digital model of the hydraulic structure and the surrounding environment. The model is divided into small, interconnected cells or volumes, forming a mesh or network. The equations governing the behaviour of fluid flow are solved numerically for each cell or volume in the mesh, taking into account the properties of the fluid, the geometry of the structure, and the surrounding environment. CFD can be used to analyze the behaviour of hydraulic structures under different flow conditions, such as water flow in a channel or river, or the behaviour of water in a reservoir or dam. The technique can also be used for optimizing the design of hydraulic structures and predicting their performance over time. Overall, numerical modelling techniques such as FEM and CFD provide a powerful tool for analyzing the behaviour of hydraulic structures under different loading conditions and for optimizing their design and performance. However, these techniques should be used in conjunction with experimental methods and field observations to ensure accurate and reliable analysis.

3.2. Integration of Finite Element Method

Integration is a critical component of the Finite Element Method (FEM) modelling process. It involves the numerical integration of the equations governing the behaviour of each element in the structure. The first step in the integration process is to subdivide the element into smaller segments. Each segment is defined by a set of nodes and a corresponding set of shape functions. The shape functions describe the behaviour of the element within the segment. Once the element is subdivided, the equations governing the behaviour of each segment are integrated numerically. This is typically done using quadrature integration, which involves approximating the integral using a finite number of

sample points. The sample points are chosen based on the order of the shape functions used to describe the behaviour of the element. The higher the order of the shape functions, the more sample points are required to achieve an accurate approximation. After the sample points are selected, the integrals are evaluated numerically using the sample points and corresponding weights. This involves multiplying the values of the shape functions and the integrand at each sample point by the corresponding weight and summing the results.

The numerical integration process is repeated for each segment of the element, and the results are combined to obtain the overall behaviour of the element. This process is repeated for each element in the structure, and the results are combined to obtain the overall behaviour of the entire structure.

Finite Element Method (FEM) is a powerful numerical modelling technique used to analyze and optimize the design of hydraulic structures. FEM can be used to analyze the stresses within hydraulic structures under different loading conditions. This can help engineers identify potential failure points and optimize the design of the structure to minimize stress concentrations. FEM can also be used to analyze the deformation of hydraulic structures under different loading conditions. This can help engineers optimize the design of the structure to minimize deformations and ensure that it remains stable and functional. FEM can be used to analyze the fatigue life of hydraulic structures, which is important for ensuring that the structure remains safe and functional over its expected service life. FEM can be used to analyze the dynamic behaviour of hydraulic structures under different loading conditions, such as earthquakes or high winds. This can help engineers optimize the design of the structure to ensure that it can withstand these types of extreme events. Fluid-structure interaction analysis: FEM can also be used to analyze the interaction between hydraulic structures and the fluid flowing through them. This can help engineers optimize the design of the structure to minimize turbulence and ensure that it operates efficiently.

4. Data Collection for Finite Element methods

Data collection is a critical aspect of Finite Element Method (FEM) modelling, as accurate and reliable input data is essential for obtaining accurate and reliable results.

The material properties of the components that make up the hydraulic structure, such as the modulus of elasticity and Poisson's ratio, are essential for accurately modelling the behaviour of the structure under different loading conditions. The geometric properties of the hydraulic structure, such as its length, width, and thickness, are also essential for accurately modelling its behaviour. The boundary conditions of the hydraulic structure, such as the type and magnitude of the loads applied, are critical for accurately modelling the behaviour of the structure. The density of the mesh used in the FEM model is also important for obtaining accurate results. A finer mesh can provide more accurate results, but it also increases the computational complexity of the model. Environmental factors, such as temperature and humidity, can also affect the behaviour of hydraulic structures and should be taken into account during data collection. Overall, accurate and reliable data collection is essential for obtaining accurate and reliable FEM results. Engineers should use a combination of experimental data, field observations, and numerical simulations to collect the necessary data and validate the accuracy of the FEM model.

5. Discussion

This article is a review note of already existing selective literature, no practical or experimental assessments were done to complete this study; hence this is the limitation of the current study. FEM is instrumental in performing failure analysis of hydraulic structures. By simulating extreme loading scenarios, such as flash floods, overtopping, or breach conditions, engineers can predict how and when a failure might occur. This analysis aids in the development of risk assessments and mitigation strategies to enhance the safety and reliability of hydraulic installations. Fluid-structure interaction problems often involve nonlinear behaviour due to large displacements, material yielding, or turbulence in fluid flow. Accurately capturing these nonlinear effects requires sophisticated modelling techniques and computational resources, which can complicate the analysis. Hydraulic structures are frequently subjected to dynamic loads resulting from waves, seismic activity, or water surges [37]. Capturing the interaction between these dynamic forces and the structural response necessitates advanced dynamic analysis techniques within the FEM framework. The quality of the mesh can significantly impact the accuracy of FEM results. For complex geometries and fluid dynamics, generating a high-quality mesh that accurately captures all features while maintaining computational efficiency poses a challenge. High-fidelity FEM simulations involving fluid-structure interaction can be computationally intensive, requiring extensive resources. As model complexity increases, the need for parallel computing or high-performance computing (HPC) systems becomes essential to manage simulation times [38]. Recent advancements in computational techniques are enhancing the application of FEM in hydraulic structural engineering i.e. developments in coupled computational fluid dynamics (CFD) and FEM.

6. Conclusion

Hydraulic structural engineering is a rapidly evolving field, driven by the demand for resilient, sustainable infrastructure. Advances in numerical modelling techniques, particularly the Finite Element Method (FEM), have enabled engineers to optimize the design of hydraulic structures and ensure their safety and performance under different loading conditions. FEM can provide valuable insights into the stresses, deformations, fatigue life, dynamic behaviour, and fluid-structure interactions of hydraulic structures, allowing engineers to optimize their design and enhance their efficiency. Furthermore, recent research has focused on developing non-destructive testing methods, innovative repair and retrofitting techniques, and sustainable design strategies to improve the maintenance and rehabilitation of hydraulic structures. The advancements in FEM and hydraulic structural engineering have contributed significantly to the development of safer, more efficient, and sustainable infrastructure. Future research efforts should focus on developing more resilient and adaptive hydraulic structures that can withstand extreme events, integrating new technologies, and promoting sustainable design practices. By addressing these challenges and opportunities, we can ensure the longevity and performance of hydraulic structures and support sustainable development for generations to come.

Competing Interests: The authors declare that they have no known competing financial interests or personal relationships that could have appeared to influence the work reported in this paper.

Author Contribution Statement: S.S, Y.Q and M.A.R conceived the idea and designed the research; Analyzed and interpreted the data and wrote the paper.

Funding Statement: This research did not receive any specific grant from funding agencies in the public, commercial, or not-for-profit sectors.

Consent to Publish: All authors agreed to publish a version of the manuscript in Journal of Engineering, Science and Technological Trends

Acknowledgement: The authors are thankful to the editor and reviewers for their valuable suggestions to improve the quality and presentation of the paper.

References

1. Felder, S., et al., *Hydraulic Structures at a Crossroads Towards the SDGs.* 2021.
2. Erpicum, S., et al., *Hydraulic structures engineering: An evolving science in a changing world.* Wiley Interdisciplinary Reviews: Water, 2021. **8**(2): p. e1505.
3. Yihong, Z. and J. Afzal. *An IoT-Based Mechanism for Monitoring Dam Structures*. in *Proceedings of the International Conference on Computing & Emerging Technologies (ICCET), Lahore, Pakistan*. 2023.
4. Chanson, H., *Hydraulics of stepped chutes and spillways*. 2002: CRC Press.
5. Novak, P., et al., *Hydraulic structures*. 2017: CRC Press.
6. Mitra, S. and K. Sinhamahapatra, *2D simulation of fluid-structure interaction using finite element method.* Finite Elements in Analysis and Design, 2008. **45**(1): p. 52-59.
7. Afzal, J., W. Lumeng, and M. Aslam, *Assessment of tolerance, harmony and coexistence: a study on university students in Government College University, Faisalabad.* Siazga Research Journal, 2022. **1**(1): p. 06-10.
8. Laminou, L.M., Z. Liu, and X. Chen, *Extreme events design and mitigation methods: A review*. Civil Engineering Journal, 2019. **5**(6): p. 1424-1439.
9. Wu, Y., et al., *Consolidation analysis of Nuozhadu high earth-rockfill dam based on the coupling of seepage and stress-deformation physical state.* International Journal of Geomechanics, 2016. **16**(3): p. 04015085.
10. Nishtara, Z. and J. Afzalb, *Seq2Seq-Based-Day-Ahead Scheduling for SCUC in Islanded Power Systems with Limited Intermittent Generation.* Journal of Engineering, Science and Technological Trends, 2024. **1**(1): p. 43-50.
11. Zhu, P., et al., *A novel sensitivity analysis method in structural performance of hydraulic press.* Mathematical Problems in Engineering, 2012. **2012**(1): p. 647127.
12. Afzal, J., M. Albassam, and M. Aslam, *Enhancing dam safety analysis through neutrosophic thermal analysis.* Advances and Applications in Discrete Mathematics, 2024. **41**(6): p. 477-492.
13. David Müzel, S., et al., *Application of the finite element method in the analysis of composite materials: A review*. Polymers, 2020. **12**(4): p. 818.
14. Xiang, X., et al., *Urban water resource management for sustainable environment planning using artificial intelligence techniques.* Environmental Impact Assessment Review, 2021. **86**: p. 106515.
15. Afzal, J., et al., *Effects of dam on temperature, humidity and precipitation of surrounding area: a case study of Gomal Zam Dam in Pakistan.* Environmental Science and Pollution Research, 2023. **30**(6): p. 14592-14603.
16. Amran, M., et al., *Recent trends in ultra-high performance concrete (UHPC): Current status, challenges, and future prospects.* Construction and Building Materials, 2022. **352**: p. 129029.
17. Afzal, J., et al., *A study on thermal analysis of under-construction concrete dam.* Case Studies in Construction Materials, 2022. **17**: p. e01206.
18. Wang, M., et al., *Recent progress of CFD applications in PWR thermal hydraulics study and future directions.* Annals of Nuclear Energy, 2021. **150**: p. 107836.
19. Afzal, J., et al., *A complex wireless sensors model (CWSM) for real time monitoring of dam temperature.* Heliyon, 2023. **9**(2).
20. Lu, Y., *Composites for hydraulic structures: a review*. 2018: West Virginia University.
21. Chen, S.-H., *Computational geomechanics and hydraulic structures*. 2019: Springer.
22. Regan, M.J. and C.D. Patel, *3D digital factories: Manufacturing centers of the new industrial age*, in *Digital Manufacturing*. 2024, Elsevier. p. 1-37.
23. Perricone, V., et al., *Nature-based and bioinspired solutions for coastal protection: an overview among key ecosystems and a promising pathway for new functional and sustainable designs.* ICES Journal of Marine Science, 2023. **80**(5): p. 1218-1239.
24. Shoshi, U.H., A. Batool, and M.A. Afzal, *Comparative Analysis of CWSM Model from Engineering Point of View.* Siazga Research Journal, 2023. **2**(2): p. 110-116.
25. Wang, H., *Numerical modeling of non-planar hydraulic fracture propagation in brittle and ductile rocks using XFEM with cohesive zone method.* Journal of Petroleum Science and Engineering, 2015. **135**: p. 127-140.
26. Afzala, J. and A. Ranib, *A Comprehensive Overview of Photon-Proton Scattering and QCD Methodology*. Journal of Engineering, Science and Technological Trends, 2024. **1**(1): p. 27-42.
27. Afzal, J. and Z. Nishtar, *A substantial study on history of climate change in south asia for sustainable development*. Journal of History and Social Sciences, 2023. **14**(1): p. 101-112.
28. Nishtar, Z. and J. Afzal, *History of emerging trends of renewable energy for sustainable development in Pakistan.* Journal of History and Social Sciences, 2023. **14**(2): p. 296-309.
29. Varas, D., R. Zaera, and J. López-Puente, *Numerical modelling of the hydrodynamic ram phenomenon.* International Journal of Impact Engineering, 2009. **36**(3): p. 363-374.
30. Athani, S.S., C. Solanki, and G. Dodagoudar, *Seepage and stability analyses of earth dam using finite element method*. Aquatic Procedia, 2015. **4**: p. 876-883.
31. Zawawi, M.H., et al. *Fluid-structure interactions study on hydraulic structures: A review*. in *AIP Conference Proceedings*. 2018. AIP Publishing.
32. Bretas, E.M., J.V. Lemos, and P.B. Lourenço, *Seismic analysis of masonry gravity dams using the discrete element method: Implementation and application.* Journal of Earthquake Engineering, 2016. **20**(2): p. 157-184.
33. Fan, S. and S. Li, *Boundary finite-element method coupling finite-element method for steady-state analyses of dam-reservoir systems.* Journal of engineering mechanics, 2008. **134**(2): p. 133-142.
34. Hui Pu, J., et al., *Evaluations of SWEs and SPH numerical modelling techniques for dam break flows.* Engineering Applications of Computational Fluid Mechanics, 2013. **7**(4): p. 544-563.
35. Amodei, D., et al., *Concrete problems in AI safety.* arXiv preprint arXiv:1606.06565, 2016.
36. Yalcin, E., *Assessing the impact of topography and land cover data resolutions on two-dimensional HEC-RAS hydrodynamic model simulations for urban flood hazard analysis.* Natural Hazards, 2020. **101**(3): p. 995-1017.
37. Toprak, S., et al., *Performance of hydraulic structures, lifelines and industrial structures during October 30, 2020 Samos-Aegean sea earthquake.* Bulletin of Earthquake Engineering, 2022. **20**(14): p. 7907-7931.
38. Fiore, S., M. Bakhouya, and W.W. Smari, *On the road to exascale: Advances in High Performance Computing and Simulations—An overview and editorial*. 2018, Elsevier. p. 450-458.

Journal of Engineering, Science and Technological Trends (JESTT)
Vol. 1, Issue 2, August 2024
DOI: https://doi.org/10.48112/jestt.v1i2c.4

Review

Review of Various Aspects of Digital Violence

Jamil Afzal[1*], Chen Yongmei[1], Adeena Fatima[2] and Anam Noor[3]

[1]Southwest University of Political Science and Law, Chongqing, China

[2]Department of Physics, University of Management & Technology, Lahore, Pakistan

[3]Department of Computer Science, University of Agriculture Faisalabad, Pakistan

* Corresponding Email: sirjamilafzal@gmail.com (J. Afzal)

Received: 03 July 2024 / Revised: 15 August 2024 / Accepted: 16 August 2024 / Published Online: 31 August 2024

ABSTRACT

This study aims to elaborate on different aspects of digital violence; several key trends and challenges are shaping the landscape of digital law. With the rise in data breaches and the misuse of personal information, governments are likely to implement more stringent data protection regulations. Innovations such as blockchain for secure data storage and AI for compliance monitoring and enforcement are expected to play significant roles. As cyber threats become more sophisticated and cross-border in nature, international cooperation and harmonization of cyber security laws will be crucial. Determining liability for cyber incidents will be an expanding area, including the responsibility of companies to protect data and the extent of government oversight.

Keywords: Cyber Terrorism; Digital Law; Digital Terrorism; Digital Violence

1. Introduction

Nowadays, a computer and the World Wide Web are an essential part of daily life and have become one of the biggest sites for the transmission of files, online commerce, and entertainment[1]. The Internet has advanced significantly since the late 1960s when it was first established as a network of Wide-Area Networks (WAN), Metropolitan Area Networks (MANs), and Local Area Networks (LANs) connected by various architectures. Routers, Switches, and other equipment all have various safety protocols and structures, and the degrees of safety also vary widely. In summary, the Internet has evolved from a small-centralized to a widely spread yet autonomous framework [2]. Nevertheless, any discovery or inquiry has advantages and disadvantages depending on how its users behave. Comparably, the information-rich portion of the Internet called the "Dark Net" is an encrypted haven for hackers and other cybercriminals that is unobserved and unaffected by law enforcement. It can only be accessible through specialized software, browsers, and protocols. Criminals and scammers frequently use such protected environments for their illicit activities, such as exchanging dangerous ideas, taking over or hacking websites, stealing private data like bank account information and related details, and taking advantage of weak points in cameras on any internet-connected device, such as a computer, to introduce malware, disrupt regular operations, and alter stored data to profit [3].

Cybercriminals thus operate in the background to damage the gadget, which results in the victim user losing important data[4]. The skill and expertise of these crooks in disguising or sheathing their malware codes to safely circumvent the latest protection measures have coincided with technological advancements [5]. Ransomware is a type of computer malware that is generated. Since multi-phase ransomware is easily accessible on the dark web in several thousand-dollar bundles, spreading the virus via it doesn't require a high level of expertise. Moreover, there are organized and well-funded gangs that operate various encrypted dark net zones and are responsible for the development of ransomware. Because the criminals constantly incorporate new technological advancements into their ransomware and employ them more quickly than others, their ransomware is incredibly successful. For example, these criminals can trick anyone by creating an authentic-looking fake website or application, marketing, or email using the well-known phenomena of social engineering and disguised [6].

This article provides a review of different aspects of digital violence. Determining liability for cyber incidents will be an

expanding area, including the responsibility of companies to protect data and the extent of government oversight. The shift in terrorist tactics from conventional methods to more intricate, technology-driven schemes necessitates a multifaceted, intelligent response that incorporates social, technological, and international measures. This study has great significance; terrorist groups often use social media, forums, and other online platforms to recruit new members and spread their ideology. They can target vulnerable individuals and communities, using sophisticated propaganda to radicalize them. Terrorist organizations use encrypted messaging apps, emails, and other digital communication tools to coordinate their activities and plan attacks while avoiding detection by authorities.

2. Evolution of Ransomware

Primitive format restricts the purpose of virus design to identify a computer's weaknesses. Malware, to put it simply, is any nefarious software that can hack, steal, and spy on sensitive data while also interfering with the system's regular operations. Malware as a whole comprises, as shown in Figure 1, viruses, Trojan horses, spyware, ransomware, logic bombs, adware, rootkits, and many more. Brain A is the first malware designed to expose vulnerabilities on a PC. It was created by Pakistani developers Bait and Amjad, and it starts by infecting a floppy diskette's boot sections [7]. Subsequently, the infection method evolved to include erasing, altering, or shredding PC File Tables.

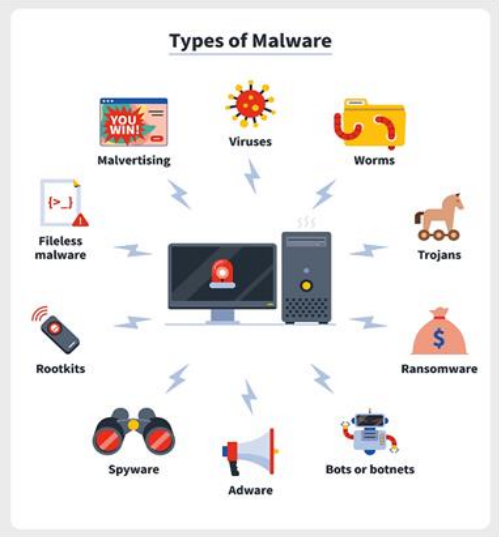

Figure 1: *Various types of Malware in Ransomware [7]*

Malware gradually began to employ polymorphism and mutation to increase its resistance to built-in security mechanisms. Years before the Internet became commercially available, in the late 1980s or early 1990s. In 1971, the first virus ever discovered was called Creeper and was created by Bob Thomas and used in the BBN Technologies Lab. After Creeper was discovered to be a worm rather than a virus, Reaper, an antivirus program, was created to prevent it from transmitting or showing messages going forward [8]. After starting with reproduction, viruses rewrote boot sectors, destroyed the File Allocation Table (FAT), and then infected the Master Boot Record (MBR). To cause further problems for the Windows operating system, the virus first infects Portable Executable (PE) files and then gains the power to kill itself. Advanced polymorphic virus variants can successfully elude antivirus software's auto-detection mechanism. Thousands of viruses infiltrated different systems throughout the world throughout this journey, but stealth viruses are more common these days [9].

Worms: To take advantage of any weakness on the device linked to the IP address, worms have an inbuilt scanning algorithm that examines the network address depicted in Figure 2. Worms also possess a greater ability to defend against security solutions. In 1988, the first worm, dubbed "Morris," appeared by mistake swamped the network with load and caused the Internet to crash [10].

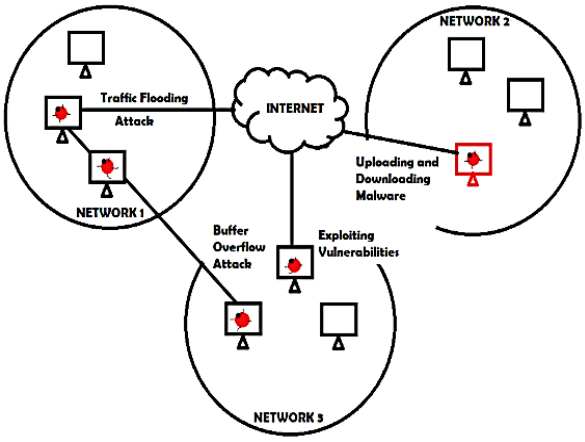

Figure 2: *Depiction of Network of worm spread in computers [7]*

Both user-mode and kernel-based mode rootkits share the same goal of altering the operating system by seizing system data and remaining undetected as demonstrated in Figure 3. Another ability of rootkits is to build a botnet made up exclusively of compromised computers, and then use that botnet to propagate other infections.

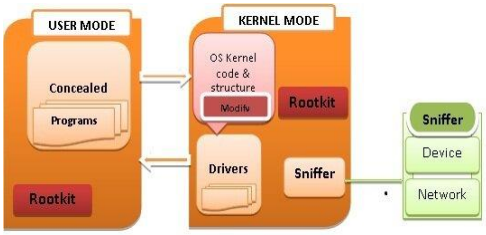

Figure 3: *ROOTKIT illustration Based On User& kernel mode [11]*

Mebroot is one such rootkit that searches for browser security holes to propagate malware. It even designates monitoring instruments that converse with hackers to pilfer any kind of victim. Its ability to return error codes or faults to the developer is an improvement that encourages debugging and fixing[12]. Trojans are a kind of malware that poses as legitimate programs, files, or apps to trick people into downloading it and unintentionally giving it access to their machines. Once installed, a trojan can carry out its intended function, which could be to corrupt, interfere with, steal from, or do other malicious things to your data or network [13]. Trojan malware, sometimes referred to as a Trojan horse or Trojan horse virus, is frequently distributed through direct messages; website downloads, and email attachments. Like viruses, they too need to be activated by the user. The distinction between trojans and malware viruses is that the former are not host-dependent, while the latter are. Unlike viruses, Trojans are unable to self-replicate. Malicious adverts that pose as trustworthy ones on websites are comparable to adware. By hacking the website, the adware may have been introduced. When an enticing advertisement is clicked, dangerous payload-containing adware is launched, causing the installation of adware from the internet or software that has been downloaded. Adware typically interferes with a

computer's operation by launching a series of windows that serve as an injector for other malware [14].

Malware like Stuxnet [15], and Flame[16] are in circulation in that era. Malicious tools written in high-level programming languages like OOC, C++, and Lua are included in this malware, which also compiles with genuine programs like Microsoft Visual Studio.

The globe suffered a severe blow in the final month of 1989 when the first ransomware attack infiltrated computer systems with a floppy diskette-based malicious program. The use of such technology in recent complex malware (from the 21st century) allows them to purposefully create generations of damage, disrupt system functionality, and steal reliable data and information. Some of them are shown in Figures 4 & 5.

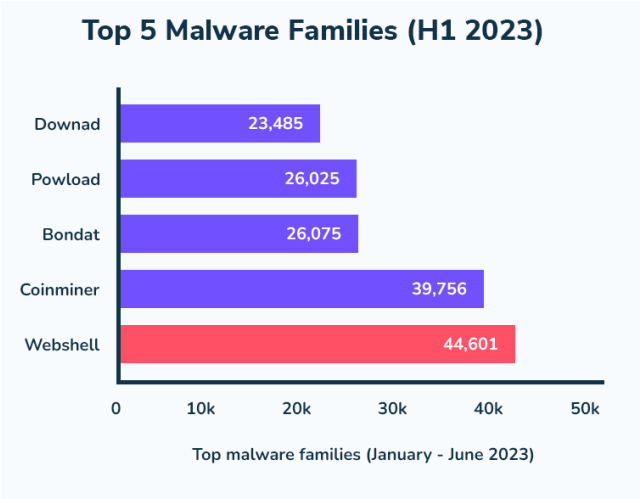

Figure 4: *Top 5 Malware Statistics in specific times span*

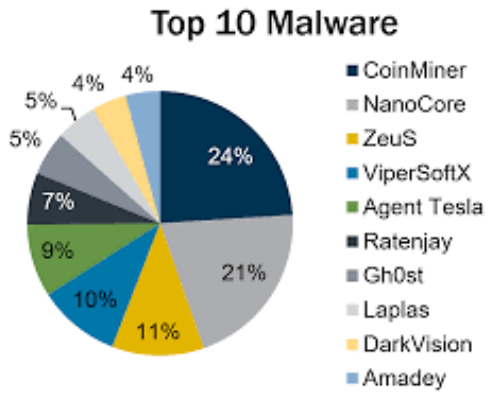

Figure 5: *Top listed Detection of Malware types in the 21st century era [17]*

3. Key Aspects of Digital Terrorism

The way terrorist groups have adapted to the digital era in light of the expanding cybertechnological milieu demonstrates a substantial and complex challenge. Terrorist organizations have changed and evolved as a result of the rapid progress of cybertechnologies, taking advantage of the opportunities presented by the internet to expand their influence, capability to operate, and impact. In the past, terrorist attacks have typically involved physical force against important targets or monuments to spread fear and further political goals. Communication's potential reach and effect were constrained by its reliance on traditional channels like print media and broadcast networks. Intelligence collecting, physical network disruption, and international collaboration were the main focuses of counterterrorism tactics to obstruct assaults and destroy organizational frameworks. Nonetheless, the advent and spread of digital technologies have drastically changed the environment in which terrorism operates. Recent Research has shown how terrorist operations in cyberspace are becoming more sophisticated and impactful, indicating a significant shift away from traditional forms of terrorism and towards more sophisticated, based on technology tactics.

For example, Kim & Yun [18] have emphasized how psychological warfare is conducted in cyberspace, where terrorist organizations actively participate in propagandistic recruiting, the rationale of acts of violence, and their spread. Buresh [19], who affirms the existence and development of digital terrorism and highlights its unique characteristics from traditional terrorism, lends additional credence to this.

Furthermore, the influence of cyberterrorism on stock market valuations, as demonstrated by Smith et al., [20] highlights the economic and societal risks associated with these terrorist operations of the digital age. The internet's ability to break through geographical boundaries, for example, enables terrorist organizations to get by censors in traditional media and spread false information to a worldwide audience directly, use social media to spread the word, encourage participation, and cultivate online terrorist networks. Digital capabilities also make it possible to produce and distribute excellent multimedia propaganda that is targeted at certain populations. A refined and convincing story is presented in video productions, interactive content, and online publications, humanizing offenders and defending violent acts.

Recognizing the quick development and accessibility of digital technology, the UN has expressed concerns over the possible exploitation of these tools by terrorist organizations. This includes worries about how the internet is being used for terrorist employment, disinformation, and organizing, as well as the abuse of increasingly sophisticated technology like cyber tools, robotics, and artificial intelligence to launch attacks or improve their capabilities. One such new and developing concern is the use of 3D printing technology in terrorism. One new facet of terrorism in the digital era is the capacity to create weapons with 3D printers, as demonstrated by events like the Halle attack, which involved handmade firearms [18]. This technology circumvents conventional approaches to arms control and acquisition, which presents serious difficulties for law enforcement and counterterrorism initiatives.

4. Historical view of Digital Terrorism

There is no general agreement on the definition of terrorism, making it a difficult topic. While historically it involved the use of force to instil fear and accomplish political objectives, there have been many differences in how it has been applied. From its original connotation of state aggression, the phrase has come to refer to non-state entities that attack governments or civilian populations. The transition from physical to digital terrorism signifies a dramatic change in the strategies and tactics used by terrorist organizations, which are distinguished by the growing use of technology to support terrorist actions, especially internet-based systems and digital communication tools Important historical events can be used to illustrate this shift from conventional techniques to the use of cybertechnologies. Each of these events demonstrated the growing influence of cybertechnologies in enabling these assaults, in addition to signalling a change in the methods and techniques used by terrorist organizations [21]. Al-Qaeda's 9/11 assaults signalled a paradigm change in terrorism, particularly concerning the use of cyber technology. This incident launched a new era in terrorist tactics and demonstrated the capability of Al-Qaeda. Following 9/11, terrorist organizations, such as Al-Qaeda, started utilizing the

internet extensively for propaganda, which was a big departure from earlier techniques. The widespread dissemination of ideas was made possible by the internet's global reach, which included the sharing of video messages from influential figures like Osama bin Laden on a variety of online venues [22]. As terrorist groups use websites, social media, and online forums, the internet has also become essential for radicalization and recruiting. These online communities provided a safe place for community development and indoctrination while maintaining anonymity, which ultimately led to radicalization.

4.1. Technology-Aided Terrorism

The Mumbai attacks of 2008, a pivotal moment in Terrorists used GPS and satellite phones for communication and navigation during the attacks, making it easier for them to travel from Karachi to Mumbai and stay in touch. This is an example of how terrorism uses cyber technology [23]. This expert use of technology for preparation and execution brought attention to the necessity of reassessing international counterterrorism plans, with a particular emphasis on the function of digital communications and real-time media coverage in such situations. It also emphasized how counterterrorism strategies must change to keep up with new technologies like massive data sets, artificial intelligence, and Blockchain [24]. The terrorists' desire and ability to use technology to improve their operations was demonstrated by the Mumbai attacks.

4.2. New Technologies and Potential Terrorism Threats

New technologies are always changing the terrain of terrorism, offering intricate difficulties and fresh chances for both terrorists and counterterrorism initiatives. The prediction and combating of threats are made more difficult by the diversification of terrorist ideology and the increase of decentralized assaults, which are frequently fueled by internet propaganda shown in Figure 6. Technology's accessibility has reduced barriers to entry and democratized terrorism, as anybody with an internet connection can launch an assault. Disinformation tactics, which make use of emerging media technologies such as AI-driven content and deepfakes, are essential in the recruitment and radicalization of terrorists. There are serious security worries over the possibility of terrorist operations abusing cutting-edge technologies like artificial intelligence (AI), drones, 3D printing, and cloud services for anything from advanced attacks to the spread of disinformation [25].

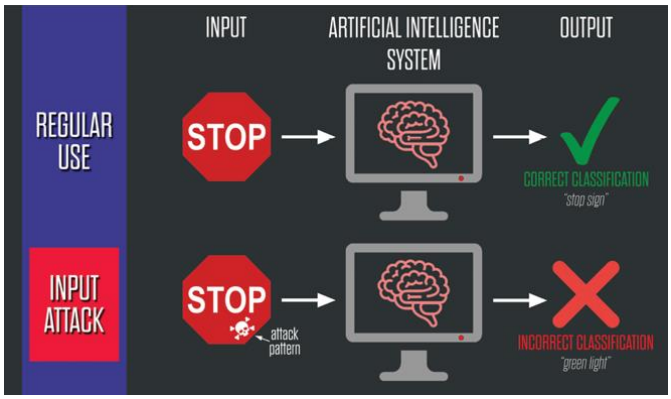

Figure 6: *The AI scam among original and morphing by cutting-edge technologies [25]*

4.3. Role of Artificial Intelligence (AI)

As our reliance on digital infrastructure grows, questions have been raised regarding AI's potential role in cyberterrorism, which includes disseminating false information and breaching important systems [26]. Because AI is so quick and effective at gathering intelligence, more control of the technology is required to stop terrorist organizations from abusing it, as depicted in Figure 7. Terrorists could use sophisticated artificial intelligence (AI) systems, such as those used in automation to map surroundings and identify impediments, to acquire information on particular targets, posing serious concerns to national security [27].

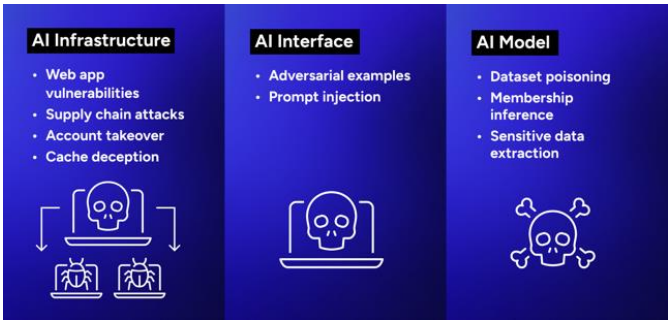

Figure 7: *Various AI Terrorism shown via different Interfaces [27]*

In contrast to the four billion dollars that was spent on research and development in 2020, the worldwide commercial sector has made significant investments in AI technology. Given the substantial cash that terrorist groups have access to, they may have access to these sophisticated artificial intelligence technologies, which are getting cheaper as a result of technology breakthroughs. This hypothetical situation highlights the necessity of strict regulation and oversight of AI technology to stop terrorist groups from using it and to maintain peace and safety around the world [27].

4.4. BROAD FAKES

The development of deep fake technology, which produces incredibly lifelike media utilizing machine learning and artificial intelligence, poses a serious risk to national security, particularly when it comes to terrorism. Deepfakes, which can produce immersive experiences, phone identities, and deceptive narratives, are abundant in this setting. While useful in programs like Google Assistant, techniques like text-to-speech and StyleGAN2 also carry a risk of being used for voice phishing and the creation of false online profiles.

Terrorist organizations in India, have incited violence, especially among young people, by using deepfake images and videos. As AI develops, more sophisticated internet disinformation may become possible. Terrorist organizations might manipulate public opinion and the chain of command by using AI-generated movies to fabricate messages from authorities. This would give them excessive power and emphasize the risks to national security posed by deep fake technology [28].

4.5. Involvement in 3D Printing

Technology development, especially in automated weapons, is changing high-skill tasks from the conflict into more mundane routines. The U.S. Army recognizes the availability of AI software and instructions that can be used with current weaponry systems online, which has resulted in developments like automated gun turrets that are put together using Raspberry Pi processors and 3D printed components. These AI-guided tools can identify and interact with targets on their own, greatly reducing the obstacles that non-state actors must overcome to improve their combat capabilities and creating new difficulties for national security.

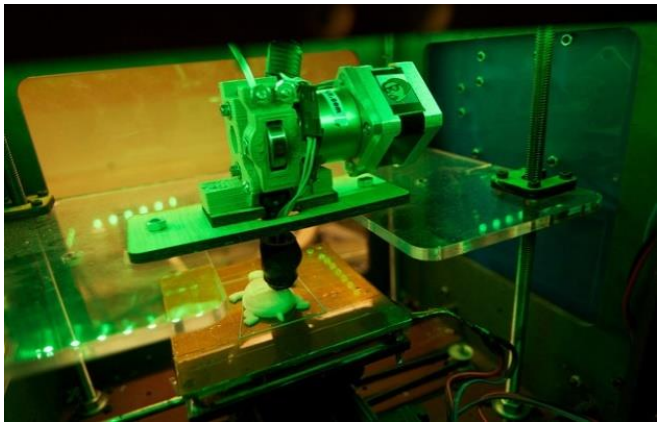

Figure 8: *Plastic Terrorism: 3D printing transformation in the security world [28]*

The contribution of 3D printing to terrorism is especially problematic because of its capacity to create weapons with advanced components quickly as shown in Figure 8. Malicious organizations can now acquire weapons without using conventional means thanks to this technology, which makes regulation and government tracking more difficult. These capabilities aren't just available to state actors; with 3D printing becoming more widely available and affordable, terrorist organizations and private citizens may also be able to use it, confounding security protocols even more. Thus, it's imperative to strike a balance between encouraging technology innovation and limiting its exploitation, necessitating the adoption of both modern technological remedies and 3-D printing regulations [29].

4.6. Could Computing

The effectiveness, availability, and data storage advantages of Cloud storage are offset by distinct difficulties in counterterrorism. Terrorist organizations may use its robust encryption, which is essential for security and privacy, to conceal communications and planning documents from law enforcement, making it difficult to track and access their data. Terrorist organizations use cloud tools to quickly share information spread disinformation and communicate across networks, dodging constant observation and necessitating a significant investment in technology and counterterrorism resources. Terrorist organizations have adapted to the digital sphere in response to stepped-up counterterrorism measures, according to Weimann and Vellante [30], who point out that these groups use anonymous content-sharing services such as Sendvid.com, and Dump. to, and JustPaste.it. These platforms provide a means of eluding conventional surveillance, enabling organizations such as ISIS to continue operating online despite social media shutdowns. The strategic redundancy in content hosting highlights how difficult it is to combat terrorism in the digital era.

4.7. DRONES

Over the past ten years, the use of weaponized drones for assault and combat missions has expanded dramatically as a result of the US successfully deploying unpiloted planes for counterterrorism missions to places like Yemen, Somalia, and Pakistan, demonstrating the advantages of lower mortality and labour costs These benefits have drawn the attention of terrorist organizations in addition to increasing the acceptance of drone technology in combat. These groups are shifting away from more conventional techniques like suicide bombs and towards the use of drones for more effective, low-risk bombing attacks. With this change, they can cause significant harm with less danger to themselves. Drone technology has advanced significantly in recent years, particularly with the addition of artificial intelligence. Because AI-driven drones are capable of performing tasks autonomously, terrorists will be able to carry out intricate, large-scale strikes effectively and quietly [31].

5. Social Context and Hyper Attacks

Terrorists can thrive on social media platforms because of their widespread accessibility and worldwide reach to groups and rebel factions to disseminate their beliefs. Ineffective content filtering guidelines and a lack of transparency, which let dangerous content stay online, are partially to blame for this spread. Large social media firms have difficulty identifying and limiting "terrorist content," as demonstrated by Facebook's difficulties moderating content based on language and cultural context differences. This problem was particularly noticeable in Myanmar, where inadequate Facebook monitoring allowed violent content to proliferate.

The lack of clarity surrounding policy enforcement on these platforms exacerbates the situation. For example, Meta Platforms, the company that owns Instagram and Facebook During the Russia-Ukraine war, the platform briefly changed its hate speech policy, permitting some posts that would typically be considered violent and in violation of established guidelines. This choice emphasizes the subjectivity of enforcing policies and the possibility of prejudice when it comes to content moderation that supports particular agendas or viewpoints Using DarkSide, Anonymity assaulted companies and religious organizations, causing instability. The group's ransomware attack on the Colonial Pipeline in 2021, which stopped the oil supply on the American East Coast, serves as an example of the numerous and serious effects of these kinds of cyberattacks. These incidents highlight the variety and sophistication with which terrorist organizations use cyberspace and digital platforms, underscoring the need for strong defences and global collaboration in the fight against terrorism in the digital age [32]. Terrorism in the digital era is a new kind of danger that goes beyond direct physical assaults to make use of the interconnection of cyberspace and have a significant socioeconomic impact. The effects of this contemporary terrorism on international relations, public opinion, and stock markets have a major impact on people, groups, and countries.

6. Conclusion

The current study was limited to the review of existing literature; this review of literature clarifies the complex and quickly changing context of violence in the digital era. The shift in violence tactics from conventional methods to more intricate, technology-driven schemes necessitates a multifaceted, intelligent response that incorporates social, technological, and international measures. In light of the study's findings, the public needs to be made aware of the dangers of violence in the digital era. This entails instructing on how to identify and report internet extremist material, recognizing disinformation and deepfakes, and encouraging critical thinking in the digital sphere. Governments, academic institutions, and internet platforms must work together to enable people to recognize and reject extremist messages, therefore lowering the danger of radicalization. International cooperation is also essential because cyberterrorism is a worldwide threat; it covers information exchange, best practices, and technical resources, working together to take down cyberterrorist networks, and creating common guidelines for controlling online areas. Collaborations with digital service providers and IT firms are crucial for controlling and keeping an eye on online content while striking a balance between speech freedom and privacy. Combating the growing threat of digital-age terrorism will require focusing counterterrorism efforts

on promoting international cooperation, improving digital literacy, and utilizing cutting-edge technology.

Competing Interests: The authors declare that they have no known competing financial interests or personal relationships that could have appeared to influence the work reported in this paper.

Ethical Issues: There are no ethical issues. All data in this paper is publicly available.

Author Contribution Statement: J.A, C.Y, A.F and A.N conceived the idea and designed the research; Analyzed and interpreted the data and wrote the paper.

Funding Statement: This research did not receive any specific grant from funding agencies in the public, commercial, or not-for-profit sectors.

Acknowledgement: The authors are thankful to the editor and reviewers for their valuable suggestions to improve the quality and presentation of the paper. The authors are also thankful to Mian Muhammad Afzal Advocate Lahore High Court, Lahore Pakistan.

References

1. Berners-Lee, T., *Long live the web.* Scientific American, 2010. **303**(6): p. 80-85.
2. Weis, A.H., *Commercialization of the Internet.* Internet Research, 1992. **2**(3): p. 7-16.
3. Jardine, E., S. Cruz, and H. Kissel, *Media coverage of darknet market closures: assessing the impact of coverage on US search and Tor use activity.* Crime, Law and Social Change, 2023. **79**(3): p. 263-289.
4. Yongmei, C. and J. Afzal, *Impact of enactment of 'the prevention of electronic crimes act, 2016'as legal support in Pakistan.* Academy of Education and Social Sciences Review, 2023. **3**(2): p. 203-212.
5. Popoola, S.I., et al. *Ransomware: Current trend, challenges, and research directions*. in *Proceedings of the World Congress on Engineering and Computer Science*. 2017.
6. Cabaj, K., M. Gregorczyk, and W. Mazurczyk, *Software-defined networking-based crypto ransomware detection using HTTP traffic characteristics.* Computers & Electrical Engineering, 2018. **66**: p. 353-368.
7. Indu, R. and A. Sharma, *Ransomware: A New Era of Digital Terrorism.* Computer, 2018. **1**(02).
8. You, I. and K. Yim. *Malware obfuscation techniques: A brief survey*. in *2010 International conference on broadband, wireless computing, communication and applications*. 2010. IEEE.
9. Pathak, P. and Y.M. Nanded, *A dangerous trend of cybercrime: ransomware growing challenge.* International Journal of Advanced Research in Computer Engineering & Technology (IJARCET), 2016. **5**(2): p. 371-373.
10. Liska, A. and T. Gallo, *Ransomware: Defending against digital extortion*. 2016: " O'Reilly Media, Inc.".
11. Kim, S., et al., *A Brief Survey on Rootkit Techniques in Malicious Codes.* J. Internet Serv. Inf. Secur., 2012. **2**(3/4): p. 134-147.
12. Milošević, N., *History of malware.* arXiv preprint arXiv:1302.5392, 2013.
13. Savage, K., P. Coogan, and H. Lau, *The evolution of ransomware, symantec security response.* Symantec Corporation, Mountain View, CA, 2015.
14. Rajesh, B., Y. Reddy, and B.D.K. Reddy, *A survey paper on malicious computer worms.* International Journal of Advanced Research in Computer Science and Technology, 2015. **3**(2): p. 161-167.
15. Kerr, P.K., J. Rollins, and C.A. Theohary, *The stuxnet computer worm: Harbinger of an emerging warfare capability*. 2010: Congressional Research Service Washington, DC.
16. Zhioua, S. *The middle east under malware attack dissecting cyber weapons*. in *2013 IEEE 33rd International Conference on Distributed Computing Systems Workshops*. 2013. IEEE.
17. Yong Wong, M., et al. *An inside look into the practice of malware analysis*. in *Proceedings of the 2021 ACM SIGSAC Conference on Computer and Communications Security*. 2021.
18. Adigwe, C.S., et al., *The evolution of terrorism in the digital age: Investigating the adaptation of terrorist groups to cyber technologies for recruitment, propaganda, and cyberattacks.* Propaganda, and Cyberattacks (February 20, 2024), 2024.
19. Buresh, D.L., *Does digital terrorism really exist.* Journal of Advanced Forensic Sciences, 2020. **1**(1): p. 18.
20. Smith, K.T., et al., *Cyber terrorism cases and stock market valuation effects.* Information & Computer Security, 2023. **31**(4): p. 385-403.
21. Abalaka, A., O. Olaniyi, and O.O. Adebiyi, *Understanding and overcoming the limitations to strategy execution in hotels within the small and medium enterprises sector.* Available at SSRN 4614043, 2023.
22. Oladoyinbo, T.O., et al., *Evaluating and establishing baseline security requirements in cloud computing: an enterprise risk management approach.* Available at SSRN 4612909, 2023.
23. Olaniyi, O., et al., *Harnessing predictive analytics for strategic foresight: a comprehensive review of techniques and applications in transforming raw data to actionable insights.* Available at SSRN 4635189, 2023.
24. Khan, F.A., et al., *AI-Driven Counter-Terrorism: Enhancing Global Security Through Advanced Predictive Analytics.* IEEE Access, 2023. **11**: p. 135864-135879.
25. Giantas, D. and D. Stergiou, *From Terrorism to Cyber-Terrorism: the case of ISIS.* Available at SSRN 3135927, 2018.
26. Afzal, J. and C. Yongmei, *Federal and provincial legislation regarding 'Right to Information'for good governance in Pakistan.* Discover Global Society, 2023. **1**(1): p. 12.
27. Trifunović, D., *Cybersecurity–virtual space as an area for covert terrorist activities of radical islamists.* Teme-Časopis za Društvene Nauke, 2021. **45**(1): p. 95-109.
28. Olabanji, S.O., et al., *AI for Identity and Access Management (IAM) in the cloud: Exploring the potential of artificial intelligence to improve user authentication, authorization, and access control within cloud-based systems.* Authorization, and Access Control within Cloud-Based Systems (January 25, 2024), 2024.
29. Olaniyi, O., O.O. Olaoye, and O.J. Okunleye, *Effects of Information Governance (IG) on profitability in the Nigerian banking sector.* Asian Journal of Economics, Business and Accounting, 2023. **23**(18): p. 22-35.
30. Weimann, G. and A. Vellante, *The Dead Drops of Online Terrorism.* Perspectives on Terrorism, 2021. **15**(4): p. 39-53.
31. Adigwe, C.S., et al., *Critical analysis of innovative leadership through effective data analytics: Exploring trends in business analysis, finance, marketing, and information technology.* Asian Journal of Economics, Business and Accounting, 2023. **23**(22).
32. Milmo, D., *Google Engineer Warns It Could Lose out to Open-Source Technology in AI Race*. 2023.

Journal of Engineering, Science and Technological Trends (JESTT)
Vol. 1, Issue 2, August 2024
DOI: https://doi.org/10.48112/jestt.v1i2c.5

Article

Improved Solar Power Prediction Using CNN-LSTM Models for Optimized Smart Grid Performance

Aamina Ahsan[1], Ahsan Zafar[2*], Muhammad Adeel Afzal[3], Mubashar Javed[4], Daniyal Zafar[5] and Mubashar Ali[6]

[1]Advanced Control System Research Group, Flinders University, Clovelly Park, Australia

[2]School of Electrical and Information Engineering, Tianjin University, Tianjin, China

[3]School of Economics and Management Science, China Three Gorges University, Yichang, China

[4]Department of Electrical and Computer Engineering, COMSATS University, Islamabad, Pakistan

[5]Faculty of Engineering, Abasyn University, Peshawar, Pakistan

[6]Department of Physics, University of Education, Lahore, Pakistan

* Corresponding Email: ahsanuetp@hotmail.com (A. Zafar)

Received: 05 July 2024 / Revised: 17 August 2024 / Accepted: 18 August 2024 / Published Online: 31 August 2024

ABSTRACT

During the fourth energy revolution, the integration of Artificial Intelligence (AI) across various technological fields is critical to meet rising energy demands and address the depletion of fossil fuel reserves, leading to the adoption of smart grids. This study aims to enhance power generation capacity and minimize losses in smart grids by accurately predicting parameters. Traditional power grid stations transitioning to smart grids require precise parameter predictions. To achieve this, we employed AI-based machine learning models, specifically Random Forest (RF) and Long Short-Term Memory (LSTM), to predict the parameters of a solar power plant. After initial analysis through graphical visualization, we further refined the LSTM model using an advanced technique: Convolutional Neural Network (CNN-LSTM). Comparative results indicate that the CNN-LSTM model outperforms both the LSTM and RF models. For daily power generation, the CNN-LSTM achieved the lowest Mean Absolute Error (MAE) of 0.1335 and Mean Squared Error (MSE) of 0.0497. Consequently, the application of AI in this study significantly improves the accuracy of parameter prediction, enhancing the performance of basic machine learning models. This advancement supports the development of a robust and efficient power system that reduces power losses and boosts production capacity within the framework of smart grids.

Keywords*:* Convolutional Neural Network; Long Short-Term Memory; Machine Learning; Solar Power; Renewable Energy

1. Introduction

Renewable energy is becoming increasingly critical as fossil fuel resources continue to dwindle. Integrating green energy sources into smart grids is essential to maintain a reliable and efficient electricity supply. Achieving this integration necessitates the use of advanced technologies like artificial intelligence (AI) [1]. Among renewable sources, solar power plants are significant contributors to meeting energy demands, generating electricity daily for national grids [2]. However, accurately predicting energy generation in solar facilities is challenging [3]. Although many established techniques exist for forecasting power generation, improving their accuracy remains a priority [4]. Recent research has utilized various machine learning (ML) models derived from diverse energy plants, demonstrating success in predicting numerous factors [5]. For instance, the LSTM model has shown lower error rates than other time-series forecasting models like Linear Regression, ARIMA, and SARIMA for predicting photovoltaic (PV) power generation output [8]. However, these models still require fine-tuning and ensemble techniques to enhance efficiency.

Machine learning models have been widely implemented not only in smart grid applications but also in energy storage, frequency modulation, and voltage stability, among other industrial and medical applications [9],[10],[11],[12]. In the medical field, a

novel deep-learning method was developed to recover high-quality cardiac MR images. This method effectively models the recurrence of iterative reconstruction stages and learns spatio-temporal dependencies, although it is limited to cardiac MR images and lacks interpretability analysis [13]. The CNN-LSTM hybrid model has demonstrated superior performance in predicting PV farm variables [14]. Despite the model's advantages, data availability and quality remain significant challenges. Similarly, the proposed CNN-LSTM model outperforms traditional ML and single deep learning models in precision, and stability, as evaluated by error metrics like MAE, MAPE, and RMSE [15]. A hybrid framework combining a CNN for local correlations, an A-LSTM network for nonlinear time-series characteristics, and an Auto-Regression model for linear time-series characteristics has shown superior accuracy in forecasting power generation from multiple renewable energy sources [16].

In weather forecasting, deep learning encoder-decoder architectures have been employed to enhance the prediction of tropical cyclone tracks and intensity. The HurriCast structure utilizes multiple ML encoder-decoder methods and data sources to achieve comparable accuracy to operational forecast models, though it is limited to specific regions and a 24-hour anticipation period [17]. Similarly, a comprehensible dam movement prediction model using a mixed attention mechanism LSTM (MAM-LSTM) adaptively selects influential factors and extracts key time segments, providing physical interpretation through the measurement and display of interest weights [18]. However, the practical application of ML models in this field faces challenges like static modelling methods and a lack of adaptive differentiation of segments and influencing factors [19]. For dynamic energy prediction at thermal energy facilities, a hybrid ML encoder-decoder architecture has been used, focusing on a new model based on physics architecture. This model demonstrates the highest accuracy in predicting heat collected by steam and water in a boiler, although further work is needed to expand the dataset and models investigated [20]. A comparison with LSTM auto-encoder models has shown that the latter are superior, albeit with a slightly higher RMSE [21].

Studies utilizing computer vision algorithms alongside ML techniques have successfully estimated wind turbine angular velocity and extracted acceptable data structures for compression, with autoencoders outperforming other feature extraction methods [22],[23]. Autoencoder techniques have also been used to accurately forecast day-ahead solar plant output, managing uncertainties and data noise, with hybrid models outperforming existing methods [24]. Similar success has been found in forecasting photovoltaic system power output using hybrid AE-LSTM models, which demonstrate higher accuracy by identifying complex temporal patterns and relationships in the data [25-28]. The hybrid method combining LSTM neural networks and autoencoders has also shown superior predictive capabilities by capturing both temporal and spatial features in the data [30]. Finally, the LSTM autoencoder (AE) model introduced for photovoltaic power forecasting has outperformed benchmark deep learning methods in various performance measures using a dataset from a 23.40 kW PV power plant in Australia [31]. These models utilize diverse input features such as panel surface temperature, accumulated energy, solar radiation, humidity, irradiance, and past solar energy to effectively forecast solar energy generation.

Accurately predicting solar energy generation is critical for effective smart grid integration. However, due to the inherent variability and instability of solar energy production, this task is challenging. This study proposes a novel approach combining a Convolutional Neural Network (CNN) with a Long Short-Term Memory (LSTM) neural network to address this challenge. The study focuses on forecasting two vital constraints: daily power generation (DPG) and radiance (Rad). The predictive capability is achieved through an LSTM model, further enhanced using CNN LSTM techniques. The main contributions of this study are as follows:

- The proposed CNN LSTM model significantly outperforms the reference models (LSTM and RF) in forecasting solar power generation across several parameters. This innovative architecture leverages the CNN layers to extract spatial features and LSTM layers to capture temporal dependencies.
- The study employs performance metrics such as Mean Absolute Error (MAE), Mean Square Error (MSE), and Root Mean Square Error (RMSE) to evaluate the models' effectiveness. Results consistently show that the CNN LSTM model surpasses both LSTM and RF models in predicting DPG and Rad.
- Using the CNN LSTM model to anticipate solar energy production more accurately is a significant contribution. This improvement is essential for maximizing financial choices about resource allocation and PV plant operations.
- The CNN-LSTM model enhances the accuracy of parameter predictions. AI contributes to the development of a resilient and efficient power system, supporting sustainability goals.

Section 2 of the paper details the proposed methodology, outlining the structure, benefits, and limitations of the prediction models used. Section 3 presents the case study, discussing the data collection process and the nature of the data using graphical visualizations. The results and associated errors are discussed in Section 4. The study is concluded in Section 5.

2. Methodology

This study employed three machine learning models: RF, LSTM, and CNN LSTM to analyze a static time series dataset. The dataset comprised daily power output data from a large-scale solar power facility collected over one year. Preprocessing ensured the data met the criteria for a stationary time series. The dataset was divided into training, sample, and validation sets. The models were trained on the training set, and their performance was evaluated on the test set, with adjustments made to enhance precision. The models' predictions were validated and used to forecast power production for the following year. These predictions, based on the models' extrapolations from the time series data, aimed to assist solar power plant operators in resource allocation and pricing decisions. The LSTM model focused on making accurate predictions about future power generation. Incorporating AI into smart grids offers several benefits, such as improved energy management, precise power output predictions, enhanced grid stability, and better integration of renewable energy sources. This study found that adding a CNN to the LSTM model improved accuracy and reduced both MAE and MSE compared to the LSTM and RF models.

The methodology involves collecting one year's worth of real-time data from a solar farm, focusing on two key metrics: daily power generation and radiance. Each metric includes approximately 365 values, representing a year of data. Three AI techniques: RF, LSTM, and CNN LSTM were developed using

Python. The data underwent initial analysis to ensure quality and consistency, verifying numerical format without inconsistencies. The data was split, with 80% (10 months) used for training the models and 20% (two months) reserved for final predictions and visualization s. These visualizations provided graphical representations of the predicted results. Comparative analysis showed that the CNN LSTM model had lower RMSE and MAE values when applied to real-time solar farm data, indicating higher accuracy in predictions compared to the LSTM and RF models. Obtaining the forecasted visual outcomes from the models is depicted in detail in the flowchart shown in Figure 1.

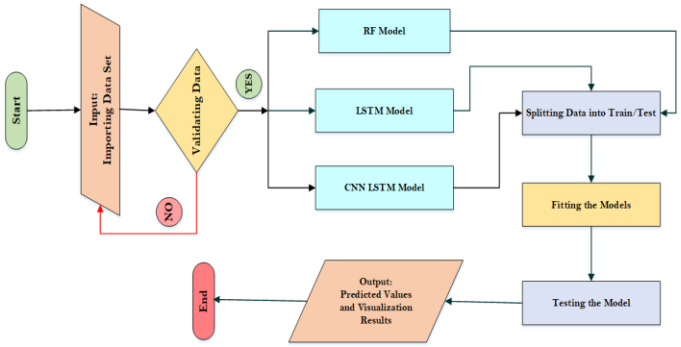

Figure 1: *Proposed Methodology Flowchart to Get Final Visualizations from LSTM, CNN LSTM and Auto-encoder LSTM.*

2.1. Functional Process of RF

The random forest model, which is well-known for its effectiveness and higher accuracy in regression when compared to other approaches, is a frequently used methodology for classification and regression in decision tree learning. The forecast is obtained by averaging the outputs of many uncorrelated decision trees that are constructed during training. The bagging approach, which fits decision trees using the Gini impurity and repeatedly chooses bootstrap samples of the training set, is used to train each tree. The outputs of all the trees are averaged, as in Equation 1, to make predictions for fresh data. Random forest as illustrated in Figure 2 produces forecasts that are more reliable and precise since it models numerous trees rather than just one.

$$Y = \frac{1}{B}\sum_{b=1}^{B} t_b(\mathrm{x}) \qquad (1)$$

Where B is the number of trees and $t_b(\mathrm{x})$ represents the prediction of each tree.

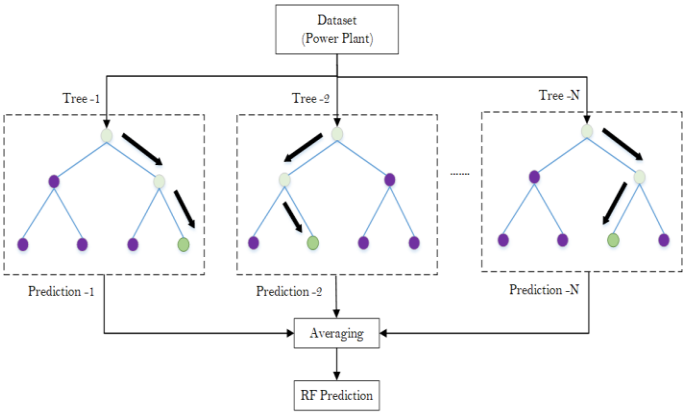

Figure 2: *RF Structure.*

A development of decision tree techniques that addresses their propensity for overfitting is random forest. Though they are prone to collecting noise, decision trees are essential in classification and regression problems. By generating an ensemble of trees trained on randomized data subsets, random forest prevents overfitting. It improves resilience and accuracy by averaging forecasts.

2.2. Functional Process of LSTM

Long Short-Term Memory (LSTM) cells are specialized units within recurrent neural networks (RNNs) designed to handle long-term dependencies in data sequences. These cells feature interconnected components that manage the selective retention or forgetting of information over time. The primary elements of an LSTM cell include the input gate, forget gate, output gate, and memory cell as shown in Figure 3. The forget gate decides which information to discard from the memory cell, applying it to remove unnecessary data. The memory cell itself stores information persistently, continuously updated by the input and forget gates and maintains its state through a self-loop connection for long-term retention. Utilizing an activation function that is sigmoid and squeezing the values obtained from the activation function that is tanh to stay within a predetermined range, the gate of output regulates the information flow from the cell of memory to the subsequent state that is hidden.

By orchestrating these elements, LSTM cells can effectively update memory, hold onto important information, eliminate unnecessary data, and produce accurate outputs, making them particularly adept at identifying long-term relationships in sequential data [8].

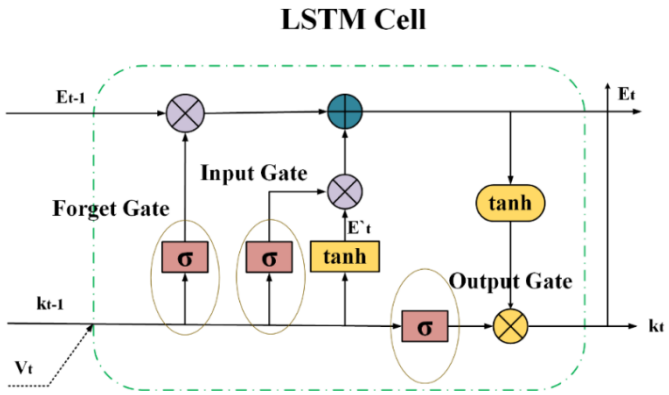

Figure 3*: Structure of LSTM.*

Three gates make up the LSTM cell structure: the gate of forget, the gate of input, and the gate of output, which controls the flow of information within the LSTM cell. Here, we provide a professional explanation of the equations mentioned in the research paper [14]: Equation (2) shows the forget gate (G_f)

$$G_f = \sigma\left\{X_f\left(k_{t-1}, v_t\right)\right\} \qquad (2)$$

Here σ is the sigma function, weighted X_f the sum of the inputs in the gate of forget, k_{t-1} is earlier step's time in a state of hidden and v_t is present input.

The gate layer of input (G_i), calculated using the function of sigmoid, selects the values that need to be updated. Equation (3), presents the tanh layer that produces new candidate (E'_t) values which might be appended to the state of the cell.

$$G_i = \sigma\{X_i(k_{t-1}, v_t)\} \quad (3)$$
$$E'_t = tanh\{X_c * (k_{t-1}, v_t)\} \quad (4)$$

The state of the cell (E_t) is modified. Equation (5) describes this update process:

$$E_t = (G_f * E_{t-1}) + E_t * E'_t \quad (5)$$

Equation (6) represents this calculation for the state of hidden (S_h).

$$G_o = \sigma\{X_o * (k_{t-1}, v_t)\} \quad (6)$$
$$S_h = G_o * tanh(E_t) \quad (7)$$

In the context of the above LSTM equations, the recurrent weights are denoted by (X_f, X_i, X_c, X_o). At time step$t$, the input, hidden state, and cell state are represented by v_t , k_t and E_t, respectively.

2.3. Functional Process of CNN LSTM:

Convolutional Neural Networks (CNNs) are structured with layers including an input layer, convolutional layers, pooling layers, fully connected layers, and an output layer, designed to directly detect visual patterns in pixel images. The CNN LSTM model, depicted in Figure 4, integrates CNN layers for feature extraction with Long Short-Term Memory (LSTM) layers for sequence prediction. This architecture is advantageous for tasks such as activity recognition, labelling images and videos, time series forecasting, and creating textual annotations from image sequences. The CNN-LSTM framework starts with an input layer for extracting features, followed by LSTM layers that capture temporal dependencies to enhance prediction. However, the CNN part extracts spatial features, while the LSTM part models sequential patterns, making the structure adept at handling datasets that are time series. This integrated approach is especially useful for forecasting time series data with intricate correlations, where understanding both spatial and temporal patterns is essential.

The flexibility of CNNs is demonstrated in various applications, including solar energy forecasting, where 1D convolution simplifies time series analysis. This versatility allows CNNs to excel in diverse tasks. The operation is defined by the equation (8)

$$z = \sigma(W * x + b) \quad (8)$$

Where z is the output feature map, $W * x$ denotes the convolution of the filter weights with the input data, and σ is the activation function. Additionally, the pooling layer's output z' is given by

$$z' = p(z) \quad (9)$$

Where z the input is the feature map and p represents the pooling operation.

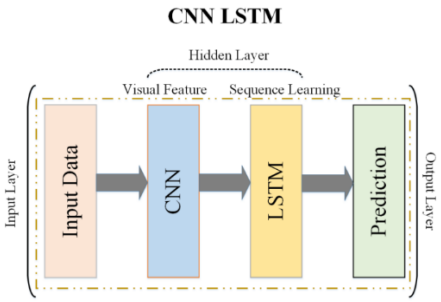

Figure 4: *Structure of CNN LSTM.*

Section 4 delves deeper into this enhanced performance, emphasizing the CNN LSTM model's efficacy in contrast to other models such as LSTM.

3. CASE STUDY

3.1 Solar Plant's Structure:

The Zhenfa Energy Group Solar PV Park, located in Punjab, Pakistan, is a notable renewable energy initiative developed and owned by Zhenfa New Energy. The construction of the Zhenfa Energy Group Solar PV Park marked a significant milestone in the country Figure 5. It shows the structure of the solar plant from where the data is collected.

This substantial project has a capacity of 100 megawatts (MW) and spans 650 acres. Operational since April 2022, the plant is equipped with over 400,000 solar panels and connects to the national grid via a 132 kV transmission line. The solar power plant, generating around 165 GWh of electricity annually, contributes to meeting Pakistan's growing energy needs while reducing reliance on fossil fuels and supporting climate change mitigation efforts.

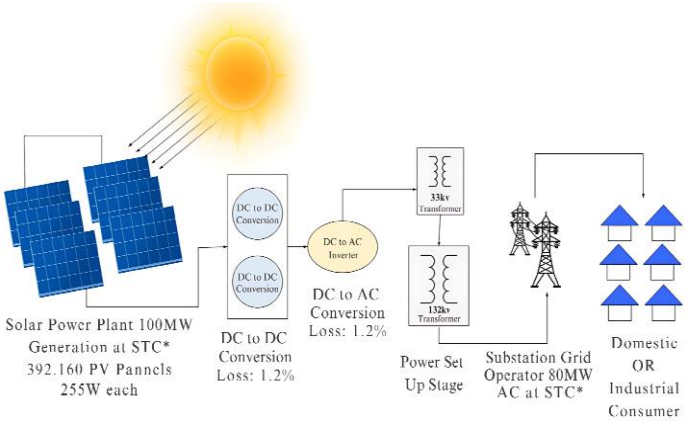

Figure 5: *Single Line Diagram to Express the Structure of Solar Plant.*

3.3. Data Analysis

The dataset for Solar Energy Variables (SEVs) comprises two categories of variables within the 100MW solar plant. In this simulation utilizing deep learning algorithms, the independent variable under consideration is the Radiance, while the dependent variable being analyzed is the Daily power generation.

Daily power generation is crucial for optimizing solar power plants, typically producing 400MW to 500MW daily. Monitored through energy meters and a SCADA system, it provides data for simulations, reflecting the plant's performance influenced by environmental factors and operational activities. This metric helps assess the plant's efficiency and its contribution to meeting energy demands and renewable energy supply. Radiance (MJ/m^2) in a solar power plant measures the solar energy received on a surface area per unit of time, crucial for evaluating energy capture efficiency. It accounts for factors like panel orientation, atmospheric conditions, and sunlight angle, directly affecting the plant's electricity generation. This metric is essential for optimizing panel alignment and overall plant performance.

Box plots provide a concise and effective method for summarizing large datasets and understanding their distribution. Figure 6 illustrates the interquartile range (Q1–Q3), median (Q2), and extreme or outlier values for three features from a large-scale

power plant: Daily Generation, and Radiance. The whiskers stretch to the least and greatest scores between a range of 1.5 times the interquartile range from Q1 and Q3, while the dimension that is vertical of the box reflects the middle 50% of the information. Relevant outliers are indicated by separate dots or circles for points of data, not within the specified range.

The heat map in Figure 7 illustrates the correlation of the three parameters in which three columns and three rows, with each cell representing the correlation coefficient between two parameters. The diagonal cells show the correlation of each parameter with itself, which is always 1. A more positive association is shown by higher numbers and lower numbers indicate a weaker negative correlation among the two variables. The values in the cells vary between 0 to 1. As an illustration, a positive correlation is denoted by a correlation factor of 1, a negative correlation is implied by a factor of -1, and no correlation is shown by a factor of 0. The range of correlation coefficients is represented by a colour bar on the right side of the heat map. The colour bar has a range between 0.6-1.0, deeper hues correspond to higher positive correlation and lighter hues to lower positive correlations.

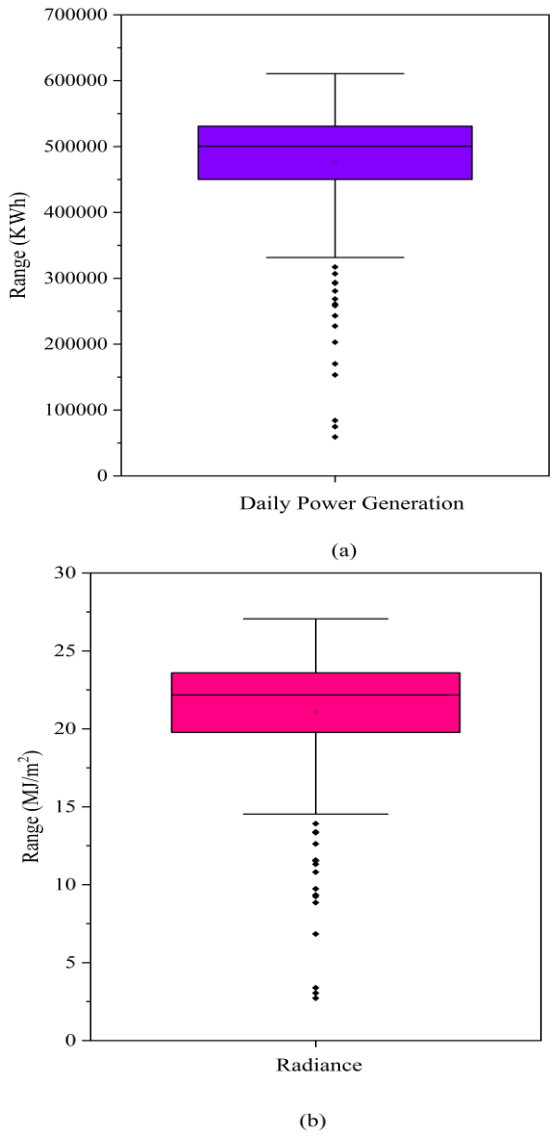

Figure 6: *Analysis of Data via Box Plot.*

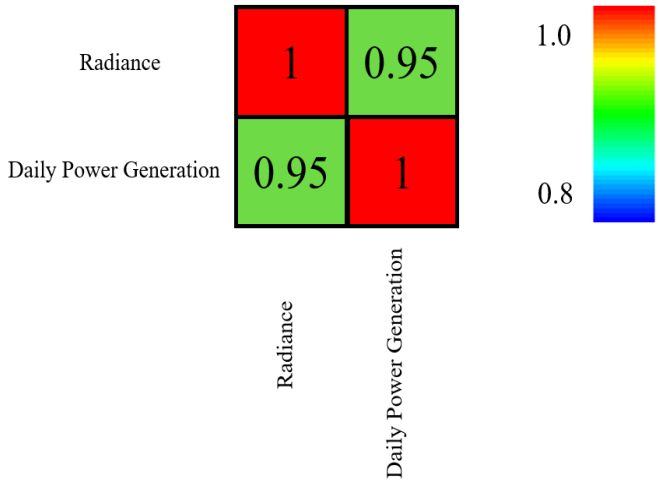

Figure 7: *Heat Map Data Analysis.*

The findings obtained from the models are presented in graphical depiction form in the following section 4.

Table 1:
Model Performance indicators.

Performance Indicator	Formula
Mean Absolute Error	$MAE = \frac{1}{N}\sum_{n=1}^{N} \lvert \overline{x_n} - x_n \rvert$
Mean Square Error	$MSE = \frac{1}{N}\sum_{n=1}^{N} (\overline{x_n} - x_n)^2$

4. Results and Discussion:

This section presents the findings derived from analyzing a year's worth of real-time data from a solar power plant, consisting of three essential parameters: “daily power generation”, and “radiance”. Our objective was to develop machine learning models for future predictions based on this dataset. After an extensive review of the literature, we opted for the RF and LSTM model due to its promising track record in similar applications. The LSTM model implementation yielded satisfactory results. However, in our pursuit of enhancing prediction accuracy, we introduced the CNN LSTM. The results are represented visually, and it is clear that the CNN LSTM model outperformed both LSTM as well as RF models, exhibiting a decreased error rate and better forecasting accuracy.

Figure 8(a & b) depicts the comparison of validation MAE among LSTM and CNN-LSTM models for the DPG and Rad parameters, the CNN-LSTM model demonstrates superior performance. For the DPG parameter, the LSTM model yields an MAE of 0.162, whereas the CNN-LSTM model achieves a lower MAE of 0.127, indicating better predictive accuracy. The difference is even more pronounced with the Rad parameter, where the LSTM model records an MAE of 0.214, compared to the significantly lower MAE of 0.115 for the CNN-LSTM model. This suggests that the CNN-LSTM model is an accurate parameter prediction.

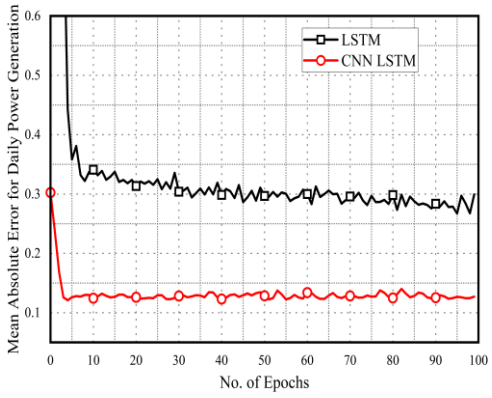

(a)

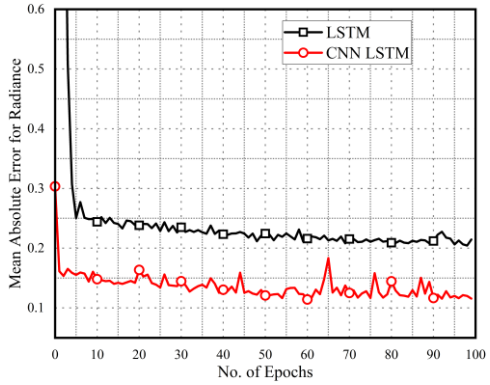

(b)

Figure 8: ***(a)***. *MAE of Daily Power Generation through LSTM & CNN LSTM and* ***(b)***. *MAE of Radiance through LSTM & CNN LSTM*

Figure 9(a & b) present the results of the loss, MAEs and MSE comparison between the RF, LSTM and the CNN LSTM model using the parameters "DPG," and "Rad," using a PV plant.

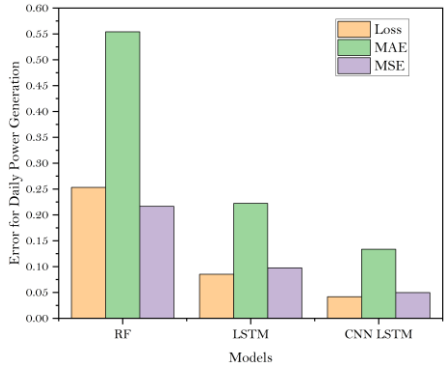

(a)

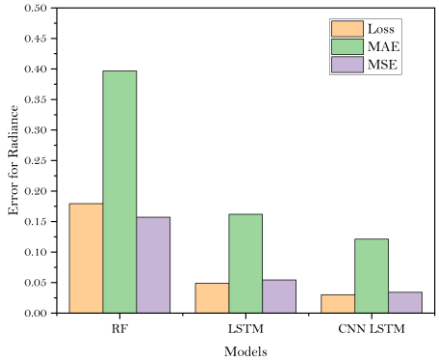

(b)

Figure 9: ***(a)***. *Error Comparison of Daily Power Generation through RF, LSTM & CNN LSTM and* ***(b)***. *Error Comparison of Radiance through RF, LSTM & CNN LSTM*

Table 2 compares the performance of three models: Random Forest (RF), Long Short-Term Memory (LSTM), and Convolutional Neural Network with LSTM (CNN LSTM) across two datasets: Daily Power Generation and Radiance. For the Daily Power Generation dataset, the CNN LSTM model outperforms both RF and LSTM, achieving the lowest Loss (0.0418), Mean Absolute Error (MAE) (0.1335), and Mean Squared Error (MSE) (0.0497). In contrast, RF shows the highest values for Loss (0.2532), MAE (0.554), and MSE (0.2165), indicating weaker performance. LSTM performs better than RF with a Loss of 0.0852, MAE of 0.2223, and MSE of 0.0976, but it still lags behind the CNN LSTM. Similarly, for the Radiance dataset, CNN LSTM again demonstrates superior performance with a Loss of 0.0301, MAE of 0.1212, and MSE of 0.0341. RF has the highest metrics, with a Loss of 0.1793, MAE of 0.3968, and MSE of 0.1571. The LSTM model performs moderately with a Loss of 0.0489, MAE of 0.16188, and MSE of 0.05427. Overall, CNN LSTM consistently provides the most accurate predictions across both datasets, highlighting its effectiveness in time-series forecasting tasks.

In Figure 10(a & b), the results of validation MSE between the LSTM and CNN LSTM models for the DPG and Rad parameters, the CNN-LSTM model consistently shows better performance. For the DPG parameter, the LSTM model achieves an MSE of 0.068, while the CNN-LSTM model improves upon this with a lower MSE of 0.055. The difference is even more significant for the Rad parameter, where the LSTM model records an MSE of 0.083, compared to the substantially lower MSE of 0.031 for the CNN-LSTM model. These results indicate that the CNN-LSTM model is more effective in reducing prediction errors.

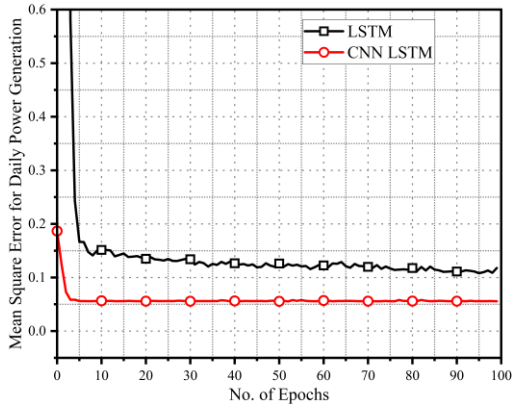

(a)

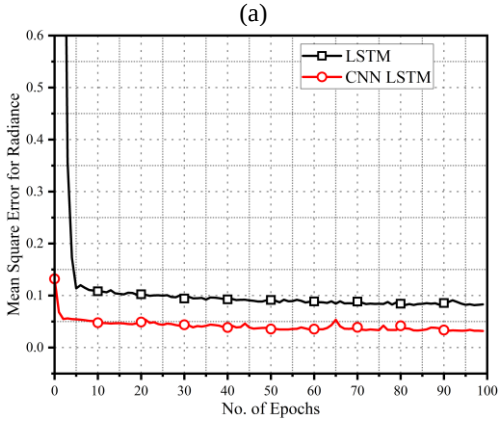

(b)

Figure 10*: ***(a)***. *MSE of Daily Power Generation through LSTM & CNN LSTM and* ***(b)***. *MSE of Daily Power Generation through LSTM and CNN LSTM*

Table 2:
Comparison Table between RF, LSTM, and CNN LSTM Results

Parameter	RF			LSTM			CNN LSTM		
	LOSS	MAE	MSE	LOSS	MAE	MSE	LOSS	MAE	MSE
Daily Power Generation	0.2532	0.554	0.2165	0.0852	0.2223	0.0976	0.0418	0.1335	0.0497
Radiance	0.1793	0.3968	0.1571	0.0489	0.16188	0.05427	0.0301	0.1212	0.0341

In addition, a close examination of each model's graphical representation shows plenty of resemblance, suggesting that the accuracy of data is higher than 95% and that none of the outliers have been found. These results provide even more evidence for the applicability and accuracy of the power plant data, offering a strong basis for further investigation and making decisions.

The practical application of parameters like daily power generation (kWh) and radiance (MJ/m²) is essential for effectively forecasting solar power plant performance. These parameters play critical roles in solar energy production, influencing multiple areas. Daily power generation is crucial for analyzing plant efficiency, planning maintenance, and estimating financial returns, making it indispensable for operators and owners. Radiance is vital for predicting energy output, tracking performance, planning maintenance, and evaluating site suitability, which together enhance the financial feasibility and dependability of solar projects. These parameters are key to maximizing efficiency, sustainability, and reliability in solar power generation. Moreover, by facilitating the production of cleaner energy and decreasing reliance on fossil fuels, these models support environmental sustainability goals. Finally, their integration into smart grids improves grid performance and stability, optimizing the use of renewable energy and advancing the development of more sustainable and efficient power systems.

Figure 11 illustrates the “Daily Power Generation (kWh)” data over a year, with the y-axis ranging from $2x10^5$ to $7x10^5$ units also the x-axis representing the days in number. This graph provides a clear visualization of the precision and performance of various ML models used for prediction. The closer the alignment between the test data and the forecast data, the more accurate the models are in predicting this parameter. By comparing the predictions from RF, LSTM, and CNN LSTM models with actual test data over 60 days, it is clear that the CNN LSTM model operates remarkably effectively. Its predictions closely match the test data with minimal discrepancies. When these models are used to forecast daily power generation over the next 10 months (300 days), the CNN LSTM model consistently outperforms the other two models. It demonstrates the lowest prediction errors compared to the actual test data, indicating its superior accuracy in forecasting daily power generation for the upcoming year. The LSTM model follows, showing better performance than the basic RF model. This suggests that the LSTM model captures more intricate patterns and dependencies in the data compared to the RF model.

In conclusion, the analysis of Figure 11 indicates that the CNN LSTM model is the most precise for predicting DPG over the next year, followed by the LSTM model. The RF model lags in terms of predictive accuracy. This information is crucial for decision-making in the energy sector, as it can help stakeholders make more informed choices regarding power generation and distribution.

Figure 12 presents the "Radiance" parameter, with values ranging from 0 to 35 MJ/m² on the y-axis and the number of days displayed on the x-axis. This figure visually showcases predictions for radiance levels over the next year using three different models: RF, LSTM, and CNN LSTM. These models are employed to forecast "Radiance" for the remaining 10 months, as shown in Figure 12. The test data graph reflects actual values from a solar power plant, while the prediction graphs display estimated values generated by the RF, LSTM, and CNN LSTM models. Over a 60-day test period, the predictions from the CNN LSTM model closely match the actual test data, with only minor deviations at certain points. A thorough analysis indicates that the CNN LSTM model consistently outperforms both the LSTM and the basic RF models. The predictions made by the CNN LSTM align closely with the test

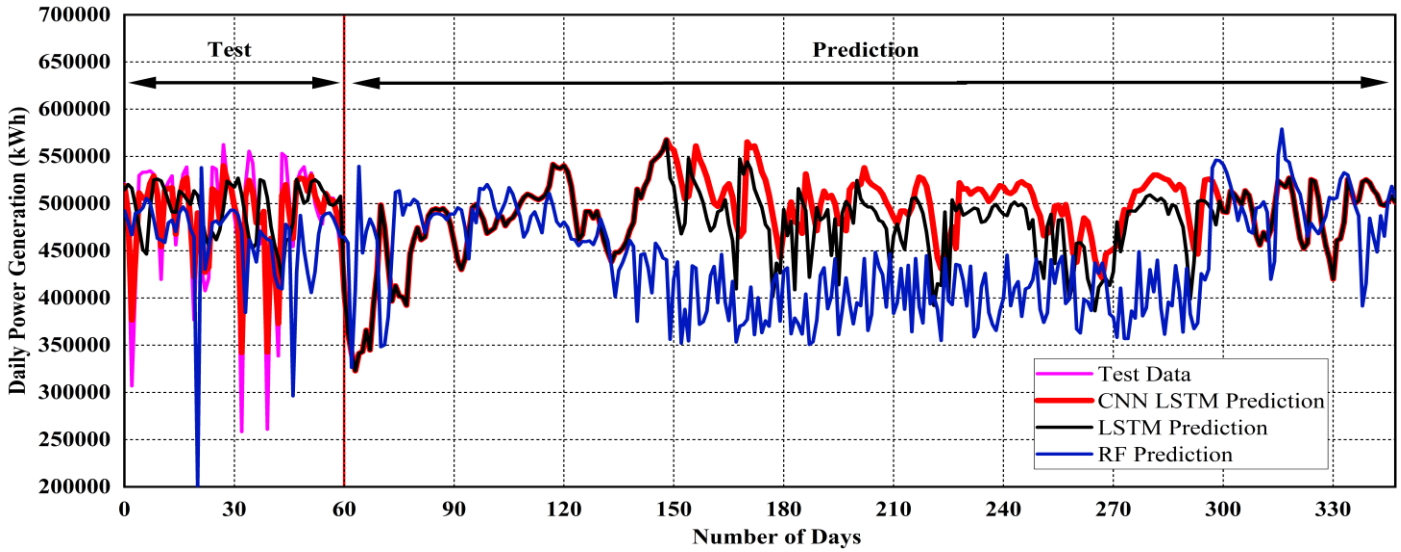

Figure 11: An Analysis of RF, LSTM, and CNN LSTM Models for Predicting Solar Plant Daily Power Generation.

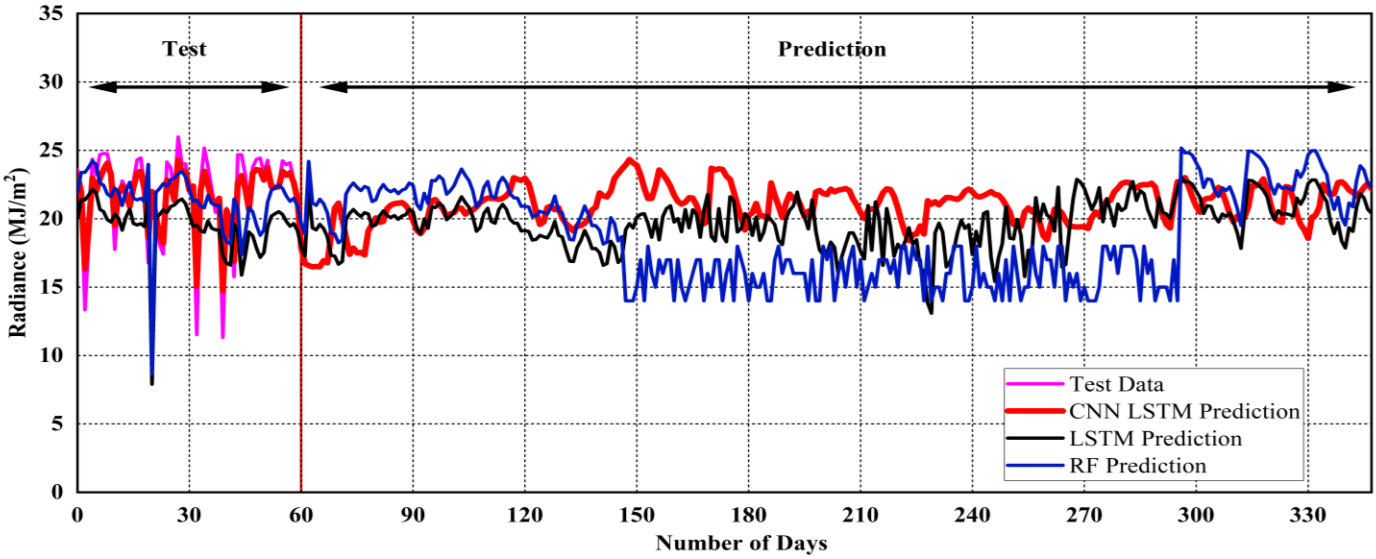

Figure 12: An Analysis of RF, LSTM, and CNN LSTM Models for Predicting Solar Plant Radiance.

data, demonstrating high accuracy in radiance forecasting. Although there are slight discrepancies, they are significantly fewer compared to those observed in the other models. The LSTM model also shows better predictive capabilities than the basic RF, although it falls slightly short of the accuracy achieved by the CNN LSTM.

These results highlight the importance of using advanced techniques, particularly the CNN LSTM, for precise radiance predictions. This data is invaluable for decision-makers in renewable energy, enabling them to make informed choices and improve their planning for radiance-related applications in the upcoming year.

5. Conclusion

In this comprehensive study, we thoroughly analyzed DPG and Rad data via a PV plant over a year. We carefully selected, extensively trained, and rigorously tested three machine learning models: RF, LSTM, and CNN LSTM to predict these crucial parameters. To evaluate the discrepancies between predicted and actual values, we used MAE and MSE as metrics. The visual representations of the results demonstrated the superiority of the CNN LSTM model over the LSTM and RF models in all scenarios. The CNN LSTM consistently exhibited reduced error scores and greater data similarity compared to the other models. Specifically, for DPG, the CNN LSTM model achieved a notably low Root Mean Square Error (RMSE) of 0.222, while the LSTM model recorded an RMSE of 0.312, and the RF model had a higher RMSE of 0.465. A similar pattern was observed for the Rad parameter, where the CNN LSTM model excelled with an RMSE of 0.184, outperforming the LSTM model (RMSE of 0.232) and the RF model (RMSE of 0.396). These results underscore the CNN LSTM's exceptional capability to accurately predict these parameters. Additionally, it's important to note that the data visualizations were based on a combination of 20% experimental data and 80% predictive data. The CNN LSTM consistently demonstrated its ability to capture underlying patterns and trends, resulting in more precise predictions across all parameters.

Further enhancing these models through hybrid or ensemble techniques could establish a solid foundation for future advancements in renewable energy technologies and their integration into existing power infrastructures. These optimized models have the potential to significantly contribute to the overall stability, reliability, and economic viability of renewable energy systems, paving the way for a greener and more sustainable future.

Data availability statement: The whole data of this research is included in this article.

Declaration of competing interest: The authors declare that they have no known competing financial interests or personal relationships that could have appeared to influence the work reported in this paper.

References

1. Pal, R., Chavhan, S., Gupta, D., Khanna, A., Padmanaban, S., Khan, B., & Rodrigues, J. J. (2021). A comprehensive review on IoT-based infrastructure for smart grid applications. *IET renewable power generation*, *15*(16), 3761-3776.
2. Qayum, M., Xu, Z., Qayyum, S., & Batool, A. (2024). New Aspect of Management Engineering: Connotation between FDI Inflow, Gender Gap, Educational Attainment and Skilled Workforce. *Journal of Engineering, Science and Technological Trends*, *1*(1), 16-26.
3. Başaran, K., Bozyiğit, F., Siano, P., Yıldırım Taşer, P., & Kılınç, D. (2020). Systematic literature review of photovoltaic output power forecasting. *IET Renewable Power Generation*, *14*(19), 3961-3973.
4. Sudharshan, K., Naveen, C., Vishnuram, P., Krishna Rao Kasagani, D. V. S., & Nastasi, B. (2022). Systematic review on impact of different irradiance forecasting techniques for solar energy prediction. *Energies*, *15*(17), 6267.
5. Abdulnabi, G. (2023). Preparation and Characterization of (CuO/TiO2/α-Fe2O3) Ternary Nanocomposite and Application in a Solar Cell. *Journal of Engineering, Science and Technological Trends*, *1*(1), 01-13.
6. Kondaiah, V. Y., Saravanan, B., Sanjeevikumar, P., & Khan, B. (2022). A review on short-term load forecasting models for micro-grid application. *The Journal of Engineering*, *2022*(7), 665-689.
7. Nishtar, Z., & Afzal, J. (2024). Seq2Seq-Based-Day-Ahead Scheduling for SCUC in Islanded Power Systems with Limited Intermittent Generation . *Journal of Engineering, Science and Technological Trends*, *1*(1), 43–50.
8. Kim, E., Akhtar, M. S., & Yang, O. B. (2023). Designing solar power generation output forecasting methods using time series algorithms. *Electric Power Systems Research*, *216*, 109073.
9. Alahmar, H. T. M. (2023). An Evaluation of Algorithms Applied to the Lattice Boltzmann Methods Technique for Segmentation of Medical Images: A Review. *Journal of Engineering, Science and Technological Trends*, *1*(1), 22–32.
10. Zafar, A. (2019). OFFSHORE WIND ENERGY CONNECTED TO HVDC SYSTEM, VSC CONTROL. *City University International Journal of Computational Analysis*, *3*(1), 29-40.
11. Shah, N., & Zafar, A. (2022). Improved Performance of Silicon-Germanium Solar Cell Based on Optimization of Layer

Thickness. *City University International Journal of Computational Analysis*, *5*(1), 1-10.
12. Farooq, M. U., Ghani, M. U., & Zafar, A. (2016, December). Survey on driving behavior and motivational factors causing aggressive driving: A case study of Peshawar, Pakistan. In *Proceedings of the 2nd International Conference on Emerging Trends in Engineering, Management & Sciences (ICETEMS-2016), Peshawar, Pakistan* (pp. 28-30).
13. Zafar, A., Che, Y., Rasool, S., Afzal, U., & Aamina, A. (2023, December). Evaluation of Machine Learning Models for Predicting Smart Grid Parameters. In *Proceedings of the 5th International Conference on Emerging Trends in Engineering, Management & Sciences (ICETEMS-2023), Peshawar, Pakistan* (pp. 15-25).
14. Jamil, I., Lucheng, H., Iqbal, S., Aurangzaib, M., Jamil, R., Kotb, H., ... & AboRas, K. M. (2023). Predictive evaluation of solar energy variables for a large-scale solar power plant based on triple deep learning forecast models. *Alexandria Engineering Journal*, *76*, 51-73.
15. Agga, A., Abbou, A., Labbadi, M., El Houm, Y., & Ali, I. H. O. (2022). CNN-LSTM: An efficient hybrid deep learning architecture for predicting short-term photovoltaic power production. *Electric Power Systems Research*, *208*, 107908.
16. Zheng, J., Du, J., Wang, B., Klemeš, J. J., Liao, Q., & Liang, Y. (2023). A hybrid framework for forecasting power generation of multiple renewable energy sources. *Renewable and Sustainable Energy Reviews*, *172*, 113046.
17. Boussioux, L., Zeng, C., Guénais, T., & Bertsimas, D. (2022). Hurricane forecasting: A novel multimodal machine learning framework. *Weather and forecasting*, *37*(6), 817-831.
18. Ren, Q., Li, M., Li, H., & Shen, Y. (2021). A novel deep learning prediction model for concrete dam displacements using interpretable mixed attention mechanism. *Advanced Engineering Informatics*, *50*, 101407.
19. Liang, J., & Tang, W. (2022). Ultra-short-term spatiotemporal forecasting of renewable resources: An attention temporal convolutional network-based approach. *IEEE Transactions on Smart Grid*, *13*(5), 3798-3812.
20. Machalek, D., Tuttle, J., Andersson, K., & Powell, K. M. (2022). Dynamic energy system modeling using hybrid physics-based and machine learning encoder–decoder models. *Energy and AI*, *9*, 100172.
21. Mukhoty, B. P., Maurya, V., & Shukla, S. K. (2019, June). Sequence to sequence deep learning models for solar irradiation forecasting. In *2019 IEEE Milan PowerTech* (pp. 1-6). IEEE.
22. Bahaghighat, M., Abedini, F., Xin, Q., Zanjireh, M. M., & Mirjalili, S. (2021). Using machine learning and computer vision to estimate the angular velocity of wind turbines in smart grids remotely. *Energy Reports*, *7*, 8561-8576.
23. Das, L., Garg, D., & Srinivasan, B. (2020). NeuralCompression: A machine learning approach to compress high frequency measurements in smart grid. *Applied Energy*, *257*, 113966.
24. Zhang, Y., Qin, C., Srivastava, A. K., Jin, C., & Sharma, R. K. (2020). Data-driven day-ahead PV estimation using autoencoder-LSTM and persistence model. *IEEE Transactions on Industry Applications*, *56*(6), 7185-7192.
25. Neo, Y. Q., Teo, T. T., Woo, W. L., Logenthiran, T., & Sharma, A. (2017, November). Forecasting of photovoltaic power using deep belief network. In *Tencon 2017-2017 IEEE Region 10 Conference* (pp. 1189-1194). IEEE.
26. Li, L. L., Cheng, P., Lin, H. C., & Dong, H. (2017). Short-term output power forecasting of photovoltaic systems based on the deep belief net. *Advances in mechanical engineering*, *9*(9), 1687814017715983.
27. Gensler, A., Henze, J., Sick, B., & Raabe, N. (2016, October). Deep Learning for solar power forecasting—An approach using AutoEncoder and LSTM Neural Networks. In *2016 IEEE international conference on systems, man, and cybernetics (SMC)* (pp. 002858-002865). IEEE.
28. Abdel-Nasser, M., & Mahmoud, K. (2019). Accurate photovoltaic power forecasting models using deep LSTM-RNN. *Neural computing and applications*, *31*, 2727-2740.
29. Zafar, A., Che, Y., Ahmed, M., Sarfraz, M., Ahmad, A., & Alibakhshikenari, M. (2023). Enhancing Power Generation Forecasting in Smart Grids using Hybrid Autoencoder Long Short-Term Memory Machine Learning Model. *IEEE Access*.
30. Said, Y., & Alanazi, A. (2023). AI-based solar energy forecasting for smart grid integration. *Neural Computing and Applications*, *35*(11), 8625-8634.
31. Zafar, A., Che, Y., Faheem, M., Abubakar, M., Ali, S., & Bhutta, M. S. (2024). Machine learning autoencoder-based parameters prediction for solar power generation systems in smart grid. *IET Smart Grid*.

Journal of Engineering, Science and Technological Trends (JESTT)
Vol. 1, Issue 2, August 2024
DOI: https://doi.org/10.48112/jestt.v1i2c.6

Perspective

Atomistic DFT simulations are promising techniques for the discovery of hydrogen storage materials

Zunaira Bibi[1,2], Mubashar Ali[3,4*], Masood Yousaf[3] and Ahsan Zafar[5]

[1]Department of physics, Govt. Islamia Graduate College, Main Saddar Dewan Road, Kasur, 55050, Pakistan

[2]University of the Punjab, Lahore, Pakistan

[3]Department of Physics, Division of Science and Technology, University of Education, Lahore, 54770, Pakistan

[4]School of Materials Science and Engineering, Beijing Institute of Technology, Beijing, China

[5]School of Electrical and Information Engineering Tianjin University, Tianjin 300072, China

* Corresponding Email: mubasharali.edu@outlook.com (M. Ali)

Received: 06 July 2024 / Revised: 21 August 2024 / Accepted: 22 August 2024 / Published Online: 31 August 2024

ABSTRACT

Efficient hydrogen storage for automobiles necessitates materials with high storage capacities, moderate dehydrogenation temperatures, and rapid kinetics for desorption and absorption. However, there are presently no known materials that exhibit all of these qualities and can be reversed. In this presentation, we provide a summary of our recent endeavours focused on creating a fundamental computational method for identifying new hydrogen storage materials. To ensure effectiveness, this technique necessitates the following essential capabilities: (i) precise forecasting of thermodynamics related to decomposition, (ii) anticipation of crystal structures for hydrides that are not yet identified, and (iii) prediction of preferred decomposition and dehydrogenation temperatures. This study demonstrates the capability of atomistic DFT modelling in identifying new materials suitable for hydrogen storage applications.

Keywords*:* Atomistic DFT simulations; Hydrogen Storage; Dehydrogenation Kinetics; Crystal Structure Identifications; Database Searching; Lattice Algebra Enumeration

1. Introduction

Hydrogen-powered vehicles require an effective method of storing hydrogen within the vehicle [1]. Presently, the existing technologies are well below the desired storage capacities, both in terms of space and weight [2],[3]. In addition to density, the thermodynamical characteristics of hydrogen insertion and release from its storing media are also of utmost importance. These thermodynamics determine the boundaries for the temperatures and pressures at which the refuelling events may take place. The realistic operational parameters of hydrogen-storing facilities for onboard vehicle applications determine the limits for the kinetics and thermodynamics that are appropriate. Currently, there is a worldwide endeavour to create a substance that can hold hydrogen with a high density in terms of weight and volume [4]. This substance should also enable fast and energy-efficient processes for adding or removing hydrogen at settings that are near room temperature.

The use of solely experimental techniques to find new materials for storing hydrogen through characterization and synthesis is both time-consuming and expensive. This is mostly owing to the large number of potential reaction routes, typically sluggish reaction rates, and the sheer volume of prospective novel compositions. An alternative method to enhance this solely empirical search would involve utilizing a precise, physics-based modelling technique that provides the thermodynamic properties of the substances involved in the process, therefore determining the enthalpies of hydrogen desorption. Here, we outline the methodology we employ. Computational screening of this kind helps expedite the identification of new crystal structures, chemical routes, and material compositions that enhance storage performance [5].

Discovering novel hydrogen storage materials using computational methods presents many substantial challenges: First, predicting the crystal structures of hydrides is another difficult task.

Second, the calculations must accurately determine the reaction energies of (de)hydriding processes quantitatively. This is necessary to obtain a precise understanding of the thermodynamics of these reactions, allowing for the confident identification of promising reactions and the elimination of thermodynamic 'dead ends'. Third, forecasting the paths of hydride decomposition and dehydrogenation temperatures: this frequently disregarded difficulty is equally crucial. The novel hydride material has the potential to solely provide the materials for a new-fangled hydrogen storage process. However, identifying the most thermodynamically favourable materials for releasing hydrogen in new storage reactions may be a challenging task. According to the target of US-DOE for 2025, the hydrides which have 5.5 gravimetric storage capacity, 40 gH_2/l volumetric storage capacity and the dehydrogenation temperature ranging from 233 to 333 K can be utilized for practical applications [3, 5].

This article presents a computational method that uses first-principles DFT simulations to find new materials for storing hydrogen. In the present article, we outline our strategies for addressing the three main obstacles in developing this technique and showcase the utility of DFT computations in the field of materials research.

2. First-principles calculations

First-principles DFT calculations are fundamental in the fields of computational materials science and quantum chemistry. They leverage the core principles of quantum mechanics to offer insights into the characteristics of materials as shown in Figure 1. The use of a plane wave basis set is a feature of these calculations providing a powerful framework for representing electronic wave functions. By expressing wave functions in terms of plane waves this method enables a precise description of the electronic structure. Additionally, pseudopotentials play a role by defining how valence electrons interact with cores simplifying computations by replacing core electrons with an effective potential. This targeted approach towards electrons enhances both computational efficiency and accuracy. While these techniques have significantly improved our understanding of materials and molecules ongoing research focuses on refining pseudopotential and basis set selections to enhance the accuracy of exchange-correlation functionals. Nonetheless, first-principles DFT calculations remain essential, for analyzing and predicting the behaviours of materials contributing significantly to technological advancements and discovery of innovative materials. The field of chemistry and materials science benefits, from a variety of DFT-based software tools as shown in Figure 2, each known for its specific strengths and applications. For example, Quantum ESPRESSO is widely recognized for its efficiency in performing structure calculations for systems [6],[7],[8],[9]. CASTEP is highly regarded for its accuracy and versatility in analyzing state and physical properties [5],[10]. Wien2k excels at modeling the structures of solids especially when studying spectroscopic properties. VASP is well respected for its ability to handle large-scale DFT calculations in the realm of materials science. These software programs along, with Gaussian, NWChem, CP2K and ADF form a collection of tools that enable researchers to explore molecular and materials systems deeply and accurately.

3. Predicting the structure of the hydrides

Predicting the energetics of the dissociation of H_2 storage compounds requires prior knowledge of the energy and crystalline structures. In the case of compounds that have not been created yet, their crystal structures cannot be determined by experimentation. Therefore, a crucial capacity of any atomistic computational method is capable of predicting the crystal structures of the compounds at the ground state energies. We provide two distinct methodologies for addressing the issue of the prediction of the crystal structures.

1. Database searching methods
2. Lattice algebra enumeration

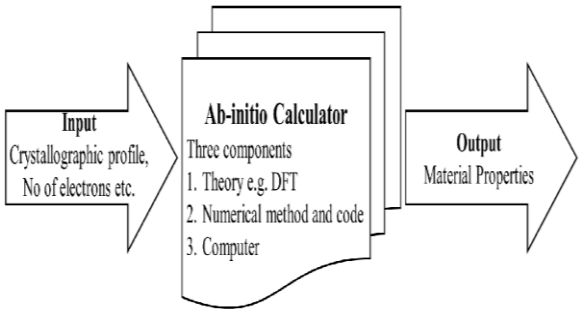

Figure 1: *A Schematic illustration of First-principles calculations using various computational codes*

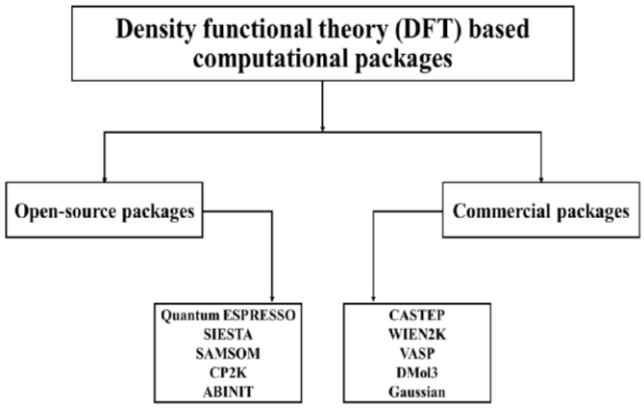

Figure 2: *Some DFT-based computational codes*

3.1. Database searching methods

This method includes looking for similar structural candidates in crystallography databases, like Materials Projects (MP), Automatic Flow for Materials Discovery (AFLOW), Crystallography Open Database (COD), Materials Cloud and Computational 2D Materials Database (C2DB) as presented in Figure 3. This is the first strategy. To begin, one generates a list of potential structures of the required compound from the MP (or another) database by making use of the structures of chemically comparable substances. This is a basic concept. In the following step, DFT computations are carried out on all possible structures to determine which structure has the lowest energy. This is followed by the computation of phonons and the verification of the structure's dynamical stability for the structure or structures with the lowest energy [11],[12]. If the compound is unstable dynamically, one has two options: either one may re-relax by moving atoms across the unstable mode(s) or one can do molecular dynamics (MD) simulations based on DFT to look for lower energy patterns. When dealing with stoichiometries that have pretty common and straightforward chemistries, it is frequently possible to discover a pretty large collection of candidate structures. This gives a substantial pool from which to sample the possible configurations of crystalline structure types. The first approach that has lately gained a lot of popularity in the field of hydride crystal structure research is the database searching strategy.

Figure 3: *Some important databases for the discovery of materials*

3.2. Lattice algebra enumeration

The aforementioned database searching strategy has proven to be highly efficient in several applications. However, it is limited in its ability to accurately anticipate entirely novel crystal structure types that have not been previously observed. Here, we provide a method called lattice algebra enumeration that overcomes this limitation. We demonstrate the application of this technique in the investigation of the composition of Li_2NH, a substance used for hydrogen storage. This approach is feasible because we can observe that the ordering problem can be converted into a binary alloy problem. This enables us to apply proven lattice algebra methods that have been developed in the alloy theory. We examine input architectures with tiny unit cells, where all N-H dimers are arranged in either antiparallel or parallel configurations along certain principal orientations. The task of enumerating various configurations of N–H dimers, given a specific orientational axis, may be conceptually equated to the binary alloy problem on a predetermined fcc lattice. This equivalence arises from the placement of N and Li atoms in a cubic fluorite structural location, resulting in the formation of a fcc sublattice by N. We categorize parallel N–H alignments as 'atoms' of type A and classify antiparallel H–N alignments as atoms of type B. By employing lattice algebra techniques derived from alloy theory, we may systematically list all conceivable organized configurations according to this lattice structure, within a predetermined cell dimension. Through a systematic examination of several organized configurations, we have discovered a stable arrangement of Li_2NH with a low energy level. This arrangement exhibits orthorhombic Pnma symmetry at a temperature of 0 K.

4. Precision of DFT computations in predicting hydrogenation enthalpies

The implementation of DFT has turned into a well-accepted and commonly used method for calculating the binding energies of complex crystals. Because the release of hydrogen reactions results in the production of H_2, and the majority of existing DFT functionals are recognized to have lower accuracy when applied to molecules and atoms compared to larger systems, it is reasonable to question the reliability of the determined DFT formation energies for screening potential hydrogen storage materials. To assess the effectiveness of using DFT for forecasting the thermodynamics of metal hydride hydrogen storage, it is necessary to have a precise grasp of the quantitative accuracy of DFT predictions.

Before that, we conducted a comprehensive investigation on ABH_3 hydride compounds containing Li and Cu [13],[14]. Figure 4 illustrates the dehydrogenation and regeneration reactions for ABH_3 hydrides. In our research, we determined the enthalpies of hydrogen release by employing the generalised gradient approximation (GGA) for the exchange-correlation function. For Cu-based hydrides, we observed that the local-density approximations (LDA) consistently produced larger hydrogenation enthalpies compared to the GGA [13]. We ascribed this difference to how the GGA and LDA models describe the H_2 molecule. Lately, we have employed this method to calculate the thermodynamics of storage reactions for a broad spectrum of hydrides. The utilization of a first-principles approach has led to the derivation of thermodynamic characteristics through calculations that exhibit a strong agreement with actual results. Additionally, we acknowledge recent research in the provided reference that examines the precision of DFT for perovskites [10]. The purpose of this research is to showcase the precision of DFT in predicting the thermodynamic parameters of dehydrogenation processes involving basic binary hydrides of alkaline earth, alkali, and early transition metals, which are generally referred to as M. Although these reactions have little practical utility for hydrogen storage, it is important to thoroughly assess the enthalpies and entropies of these reactions to verify the precision of the existing first-principles electron structure approaches. The metal hydrides undergo decomposition using a subsequent general reaction.

$$MH_p \rightarrow M + \frac{p}{2}H_2 \qquad (1)$$

A possible expression for the enthalpy (ΔH) that corresponds to equation (1) is as follows:

$$\Delta H = \frac{p}{2}\left[E_{H_2}^{tot} + E_{H_2}^{vib} + \frac{7}{2}\kappa_b T\right] + E_M^{tot} + E_M^{vib} - E_{MH_p}^{tot} - E_{MH_p}^{vib} \qquad (2)$$

Here, E^{tot} is total energy whereas E^{vib} is the vibrational energy, which is obtained from the phonon calculations. Wolverton et al [1] have utilized equation (2) for different compounds and they reported that the inclusion of vibrations enhances the accuracy of the predicted ΔH values, which are computed with PBE-GGA functionals. Furthermore, they suggested that the vibrations should be incorporated into the discovery of novel materials for hydrogen storage.

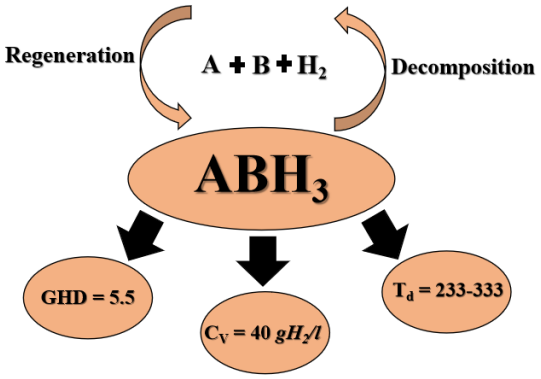

Figure 4: *A general representation of regeneration and decomposition reactions for ABH_3 hydrides.*

5. Decomposition and dehydrogenation temperatures

Decomposition and dehydrogenation temperatures play roles in the field of materials, particularly in relation, to how they impact hydrogen storage and release. These temperatures are indicators of the stability and hydrogen desorption properties of hydride

materials significantly influencing their practical use in storing hydrogen. The decomposition temperature marks the point at which a hydride material breaks down thermally releasing hydrogen gas. On the other hand, the dehydrogenation temperature signifies when the material releases hydrogen through desorption an important factor in assessing its suitability for storing and retrieving hydrogen. These temperatures vary significantly depending on the composition, structure and inherent characteristics of the hydride material being studied. Understanding and optimizing these temperatures are steps in developing effective hydrogen storage materials. Therefore, researchers are actively seeking hydride systems, with decomposition and dehydrogenation temperatures to enhance the potential of using hydrogen as an energy source. It is interesting to note that the atomistic DFT computation gives highly accurate predictions about the decomposition and dehydrogenation temperatures of the hydrides as calculated in the previous work [3-5]. We can calculate the dehydrogenation temperatures for the hydride materials by using the following equations.

$$\Delta G = \Delta H - (T_d \times \Delta S) \qquad (3)$$

Where ΔS is the change in entropy of the system and T_d is the dehydrogenation temperature for the hydrides. By increasing temperature $\Delta G \approx 0$, So, equation (3) can be modified to equation (4) as given below [15].

$$T_d = \frac{|\Delta H|}{\Delta S} \qquad (4)$$

6. Conclusion

Atomistic DFT calculations were usually limited to theoretical physicists, and may now be widely utilized in several fields of materials research that are directly applicable to industry. Additional proof of the effectiveness of this method may be observed in our recent endeavours focused on the exploration of novel materials for storing hydrogen. Currently, no material possesses the necessary combination of high storage densities, suitable dehydrogenation temperatures and cost-effectiveness required for use in onboard applications. It is necessary to develop new hydrides that have improved characteristics. Two examples of approaches for identifying ground-state crystals of novel materials were presented: one of them is database searching whereas the other is lattice algebra enumeration. These approaches are essential because the precision of any thermodynamic forecast based on fundamental principles would be influenced by the crystalline geometry of the phases being studied. Both techniques have demonstrated efficacy in detecting low-energy phases. Further study in this field is strongly recommended, particularly in situations when the available database of potential structure prototypes is limited. Overall, these qualities make DFT computing an important tool for estimating the thermodynamics of hydrogen storage processes. Nevertheless, it is crucial to acknowledge that while having favourable thermodynamics is vital, it is not enough to ensure the creation of appropriate hydrogen storage materials. The dynamics of hydrogen absorption and release will also have a significant impact and should be taken into account in any comprehensive analysis of hydrogen storage.

Data availability statement: The whole data of this research is included in this article.

Acknowledgement: The authors thank the corresponding author for conceptualization and assistance in completing this work.

Author contribution: Zunaira Bibi wrote the original draft, Mubashar Ali contributed to the conceptualization, writing, reviewing and editing of the original draft, Masood Yousaf contributed to reviewing and editing the original draft, Ahsan Zafar conducted a formal analysis of this work.

Declaration of competing interest: The authors declare that they have no known competing financial interests or personal relationships that could have appeared to influence the work reported in this paper.

References

1. Ali, M., et al. (2024). "First-principles evaluation of LiCaF3-αHα as an effective material for solid-state hydrogen storage." *Journal of Energy Storage* 83: 110731.
2. Ali, M., et al. (2024). "Effective hydrogen storage in Na2(Be/Mg)H4 hydrides: Perspective from density functional theory." *International Journal of Hydrogen Energy* 64: 329-338.
3. Ali, M., et al. (2024). "A Computational Investigation of Lithium-Based Metal Hydrides for Advanced Solid-State Hydrogen Storage." *ChemistrySelect* 9(10): e202304582.
4. Ali, M., et al. (2024). "Structural, optoelectronic and thermodynamical insights into 2H-ZrO2: A DFT investigation." *Inorganic Chemistry Communications* 160: 111891.
5. Ali, M., et al. (2024). "Enhancement of hydrogen storage characteristics of Na2CaH4 hydrides by introducing the Mg and Be dopant: A first-principles study." *International Journal of Hydrogen Energy* 70: 579-590.
6. Ali, M., et al. (2024). "An accurate prediction of electronic structure, mechanical stability and optical response of BaCuF3 fluoroperovskite for solar cell application." *Solar Energy* 267: 112199.
7. Ali, M., et al. (2024). "First-principles investigation of structural, mechanical, and optoelectronic properties of Hf2AX (A═ Al, Si and X═ C, N) MAX phases." *Journal of the American Ceramic Society* 107(4): 2679-2692.
8. Ali, M., et al. (2024). "Achieving controllable multifunctionality through layer sliding." Journal of Molecular Graphics and Modelling 126: 108638.
9. Ali, M., et al. (2023). "Controlled dynamic variation of interfacial electronic and optical properties of sodium-intercalated silicene/hBN heterostructure." *The European Physical Journal Plus* 138(12): 1151.
10. Ali, M., et al. (2024). "Physical properties and defect processes of Zr3AC2 (A= Al and Si) MAX phases: Implication for radiation tolerance." *Materials Science and Engineering: B* 308: 117619.
11. Ali, M., et al. (2023). "Layer-sliding-mediated controllable synthetic strategy for the preparation of multifunctional materials." *Materials Today Communications* 37: 107022.
12. Gupta, S. L., et al. (2024). "Ab initio studies of newly proposed zirconium based novel combinations of hydride perovskites ZrXH3 (X= Zn, Cd) as hydrogen storage applications." international journal of hydrogen energy 55: 1465-1475.
13. Mubashir, M., et al. (2024). "Computational evaluation of novel XCuH3 (X= Li, Na and K) perovskite-type hydrides for hydrogen storage applications using LDA and GGA approach." *Journal of Molecular Graphics and Modelling*: 108808.
14. Mubashir, M., et al. (2024). "Efficient hydrogen storage in LiMgF3: a first principle study." *International Journal of Hydrogen Energy* 50: 774-786.
15. Wolverton, C., et al. (2008). "Discovery of novel hydrogen storage materials: an atomic scale computational approach." *Journal of Physics: Condensed Matter* 20(6): 064228.